THE JOURNAL OF BIOLOGICAL CHEMISTRY VOL. 280, NO. 51, pp. 42375–42382, December 23, 2005

EphA2 Phosphorylates the Cytoplasmic Tail of Claudin-4 and Mediates Paracellular Permeability*

Received for publication, April 7, 2005, and in revised form, September 2, 2005 Published, JBC Papers in Press, October 18, 2005, DOI 10.1074/jbc.M503786200

Masamitsu Tanaka, Reiko Kamata, and Ryuichi Sakai[1]

From the Growth Factor Division, National Cancer Center Research Institute, 5-1-1 Tsukiji, Chuo-ku, Tokyo 104-0045, Japan

Eph receptors and ephrin ligands are widely expressed in epithelial cells and mediate cell-cell interaction. EphA2 is expressed in various cancer tissues and cell lines. Although the mechanism of action of EphA2 is unknown, its expression correlates with progression of the malignant phenotype of cancerous tissues. Here, we have shown that EphA2 modulates the localization and function of claudin-4, a constituent of tight junctions. EphA2 associates with claudin-4 via their extracellular domains. This association, in turn, leads to phosphorylation of the cytoplasmic carboxyl terminus of claudin-4 at Tyr-208. The tyrosine phosphorylation of claudin-4 attenuates association of claudin-4 with ZO-1, decreasing integration of claudin-4 into sites of cell-cell contact and enhancing paracellular permeability. These results indicate that EphA2 moderates the function of tight junctions via phosphorylation of claudin-4.

The members of the Eph receptor family can be classified into two groups based on their sequence similarity and their preferential binding to ligands tethered to the cell surface by a glycosylphosphatidyl inositol anchor (ephrin-A) or by a transmembrane domain (ephrin-B) (1–4). Although the studies of Eph receptors and ephrins have focused on their neuronal targeting and neural plasticity (5–9), they are also widely expressed in epithelial cells, and overexpression of Eph receptors and ephrins has also been reported in various tumors. In particular, the overexpression of EphA2, an Eph receptor, was shown to correlate with poor prognosis and high vascularity in these cancer tissues (10–15).

In epithelial cells, cell-cell adhesion appears to be closely connected with the function of Eph receptors. For example, E-cadherin-mediated cell-cell adhesion is required for EphA2 localization at cell contacts, and the loss of E-cadherin decreases the phosphotyrosine content of EphA2 (16, 17). In addition, disrupting signaling through some of the Eph receptors and ephrins leads to impaired cell-cell adhesion in early stage *Xenopus* embryos (18, 19).

Tight junctions locate at the most apical part of lateral membranes and serve as a paracellular barrier to restrict the movement of molecules, including ions and proteins, across cell boundaries. Claudins, a family of tetraspan transmembrane proteins containing more than 20 members, are a major constituent of tight junctions (20, 21). Carboxyl-terminal YV sequences conserved among claudin families are involved in interaction with PDZ domain-containing molecules such as ZO-1, ZO-2, ZO-3, MUPP1, and PATJ (22–24). ZO family proteins maintain plaque structures underlying tight junctions. Claudins are one of the most frequently overexpressed genes in various malignant cells (25–27). During the screening of cross-talk between Eph-ephrin family molecules and intercellular adhesion molecules, we found that EphA2 makes a complex with claudin-4, which led us to investigate whether claudin-4 is a biochemical target of EphA2.

In this study, we have described the biological interaction of EphA2 with claudin-4. Upon cell-cell contact, a tyrosine residue located in the carboxyl-terminal region of claudin-4 was phosphorylated by activated EphA2. This phosphorylation event lead to reduced association of claudin-4 with ZO-1 and decreased integration of claudin-4 into sites of cell-cell contact. Analysis of paracellular flux indicated that activation of EphA2 delayed assembly of tight junctions in Madin-Darby canine kidney (MDCK)[2] cells, and this depended on EphA2 kinase activity. These results show that, by regulating the localization and function of claudin-4, EphA2 moderates tight junction permeability.

EXPERIMENTAL PROCEDURES

Plasmids and Antibodies—Plasmids encoding full-length human EphA2 and a mutant EphA2^{K646M} were previously described (28). The Fc fusion protein expression constructs EphA2, ephrin-A1, EphB2, and ephrin-B1 were constructed using PCR-generated amplicons of the entire extracellular domain of each protein as previously described (28, 29). Mutants of EphA2, lacking either the cytoplasmic domain (EphA2-(1–563)) or the extracellular domain (EphA2-(541–977)) were constructed by tagging PCR-generated amplicons with GFP at the carboxyl or amino terminus, respectively. The plasmids encoding claudin-4 and N-ZO-1 (amino acids 1–862) were donated by S. Tsukita. Mutants of claudin-4 (Y193F, Y197F, Y208F, Y193/197F, and Y193/197/208F) and EphA2 (I94N) were generated using the Altered Sites mutagenesis system (Promega). The truncated mutants of claudin-4 shown in Fig. 2*a* were constructed by cloning PCR-generated amplicons into pEBB with the addition of the FLAG epitope tag at the carboxyl terminus. The antibodies for the FLAG (M2) and hemagglutinin (Y-11) tags were obtained from Sigma and Santa Cruz, respectively. The monoclonal antibodies for EphA2 and phosphotyrosine (4G10) were purchased from Upstate Biotechnology. The antibodies for claudin-4 and ZO-1 were purchased from ZyMed. Anti-GFP was from NacalaiTesque. Alexa Fluor-labeled secondary antibodies of anti-goat IgG, anti-rabbit IgG, and anti-mouse IgG were purchased from Molecular Probes. Fusion proteins of Eph and ephrin with the Fc region of immunoglobulin were purified by passing the culture medium of COS1 cells transfected with plasmids encoding the Fc fusion proteins through a protein A-Sepharose column as previously described (29).

Cell Culture and Transfection—HT29 colon carcinoma cells were cultured in RPMI 1640 supplemented with 10% fetal bovine serum. MDCK cells and COS1 cells were cultured in Dulbecco's modified Eagle's medium with 10% fetal bovine serum. For transient expression

* This work was supported by the Program for the Promotion of Fundamental Studies in Health Science of the Organization for Pharmaceutical Safety and Research of Japan. The costs of publication of this article were defrayed in part by the payment of page charges. This article must therefore be hereby marked "*advertisement*" in accordance with 18 U.S.C. Section 1734 solely to indicate this fact.

[1] To whom correspondence should be addressed. Tel.: 81-3-3547-5247; Fax: 81-3-3542-8170; E-mail: rsakai@gan2.res.ncc.go.jp.

[2] The abbreviations used are: MDCK, Madin-Darby canine kidney; GST, glutathione S-transferase; ECD, extracellular domain; GFP, green fluorescent protein; FITC, fluorescein isothiocyanate.

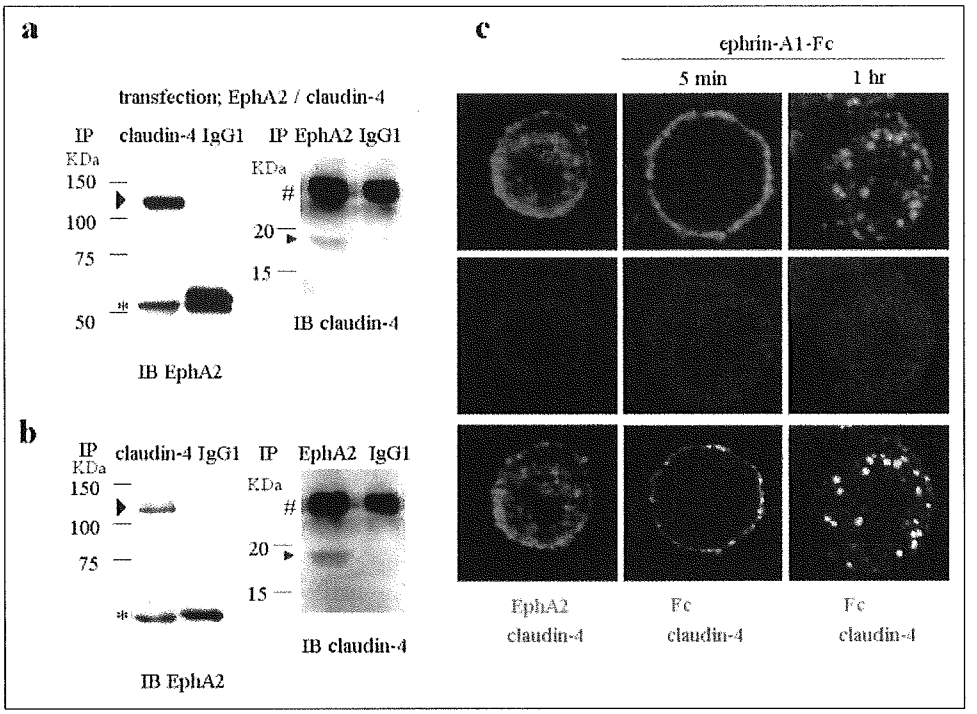

FIGURE 1. **EphA2 associates with claudin-4.** *a*, COS1 cells were transiently transfected with a plasmid encoding EphA2 together with a plasmid encoding claudin-4. Cells were lysed and immunoprecipitated (*IP*) with anti-claudin-4, anti-EphA2, or mouse IgG1 as indicated. The precipitates were subjected to immunoblotting (*IB*) with the indicated antibodies. *Arrowheads* indicate coprecipitated EphA2 (*left*) and claudin-4 (*right*). *Asterisk* and *sharp sign* indicate IgG heavy chain and light chain, respectively. *b*, EphA2 physiologically associates with claudin-4 in HT29 cells. HT29 cells were lysed and subjected to immunoprecipitation (*IP*) and immunoblotting (*IB*) with the indicated antibodies. *Arrowheads* indicate coprecipitated EphA2 (*left*) and claudin-4 (*right*). *c*, stimulation of the EphA2 receptor induces the redistribution of claudin-4. HT29 cells were untreated (*left column*) or incubated with clustered ephrin-A1-Fc for 5 min or 1 h as indicated above the middle and right columns. The cells were stained with antibodies against either EphA2 or Fc together with anti-claudin-4 as indicated at the bottom.

assays, COS1 cells were transfected with plasmid DNA using FuGENE 6 reagent (Roche Applied Science).

Generation of Adenoviruses and Adenoviral Infection—To generate recombinant adenoviruses, cDNAs encoding wild type, the K646M mutant of EphA2, or EphA2-(1–563)-GFP were subcloned into the vector pShuttle-CMV (Stratagene). They were transformed into an *Escherichia coli* strain containing the Ad5-based adenovirus vector pADEasy-1 (Stratagene). Transposition of the EphA2 cDNAs from the pShuttle-CMV into pADEasy-1 created the adenoviral vectors pAD-EphA2 (wild type, K646M, and EphA2-(1–563)-GFP) where the transgenes were under the control of the cytomegalovirus promoter. Recombinant adenoviral DNA was transfected into 293 human embryonic kidney cells to allow production of adenoviral particles. The titer of adenovirus stocks was determined by Adeno-X rapid titer kit (Clontech) according to the manufacturer's instructions. Confluent MDCK cells grown on Transwell filters or glass coverslips were infected with adenoviruses at a multiplicity of infection of 5 in medium containing 10% fetal bovine serum. After incubation for 12 h the virus-containing medium was removed and fresh medium containing 10% fetal bovine serum was added. The infected cells were used for permeability assays or immunostaining 48 h after the infection.

Immunoprecipitation and Immunoblotting—Transfected cells were harvested 48 h after transfection, and cell lysates were prepared with protease inhibitors in PLC buffer (50 mM Hepes (pH 7.5), 150 mM NaCl, 1.5 mM $MgCl_2$, 1 mM EGTA, 10% glycerol, 100 mM NaF, 1 mM Na_3VO_4, and 1% Triton X-100). The lysates were precleared by incubation with protein G-agarose (Roche Applied Science) for 1 h at 4 °C. To purify target proteins, 1 μg of monoclonal or affinity-purified polyclonal antibody was incubated with 500 μg of precleared cell lysate for 2 h at 4 °C and then precipitated with protein G-agarose for 1 h at 4 °C. Immunoprecipitates were extensively washed with PLC buffer, separated by SDS-PAGE, and subjected to immunoblotting. After blocking, blots were incubated with appropriate primary antibodies. Blots were then washed four times with TBST (150 mM NaCl, 10 mM Tris (pH 8.0), and 0.05% Tween20), incubated with horseradish peroxidase-conjugated anti-mouse or anti-rabbit whole IgG antibodies (Amersham Biosciences) for 30 min, washed, and visualized by autoradiography using chemiluminescence reagent (Western Lighting; PerkinElmer).

Cell Staining—Cells were fixed for 5 min at room temperature with 4% paraformaldehyde in phosphate-buffered saline and permeabilized for 10 min with 0.2% Triton X-100. The cells were preincubated in 2% bovine serum albumin with 5% normal serum for 0.5 h and incubated with specific primary antibodies for 1 h at room temperature. After washing, cells were incubated with Alexa-conjugated secondary antibodies (Molecular Probes) for 0.5 h at room temperature. In some experiments, membrane-bound Fc fusion proteins were stained with Alexa488-conjugated anti-mouse IgGFc for 0.5 h. Photos were taken with a Radiance 2100 confocal microscope (Bio-Rad).

In Vitro Binding Assay—The recombinant GST-tagged claudin-4 containing the second cytoplasmic domain was prepared in TKX1-competent cells (Stratagene) by transformation with pGEX4T claudin-4. Tyrosine-phosphorylated GST-claudin-4 was prepared by induction of a nonspecific tyrosine kinase in TKX1 cells according to the manufacturer's instructions. GST-tagged proteins (2.5 μg) were purified using glutathione-agarose. Each GST-tagged protein (2.5 μg) was incubated with lysate prepared from COS1 cells transfected with N-ZO-1 in PLC buffer for 4 h at 4 °C. The beads were washed four times with the same buffer, and bound proteins were separated by SDS-PAGE. Precipitated N-ZO-1 was detected by immunoblotting with anti-ZO-1 antibody.

Paracellular Permeability Assay—MDCK cells were seeded into the upper well of transwell chambers (0.4-μm pore size; Becton Dickinson Labware). After the cells reached confluence and established tight junctions, the medium of both the upper and lower wells was replaced with Hanks' balanced salt solution containing 2 mM EGTA. The extent of cell-cell contact after treatment with EGTA was confirmed by microscopic observation. The medium was replaced from calcium-free to normal growth medium with 0.5% fetal bovine serum (calcium switch), and monolayers were allowed to recover for the indicated period. FITC-dextran (M_r 3,000 or 2,000) was added to the upper well at a concentration of 10 μg/ml and incubated for 30 min. Samples were then taken from the lower compartment of the transwell chamber. The amount of

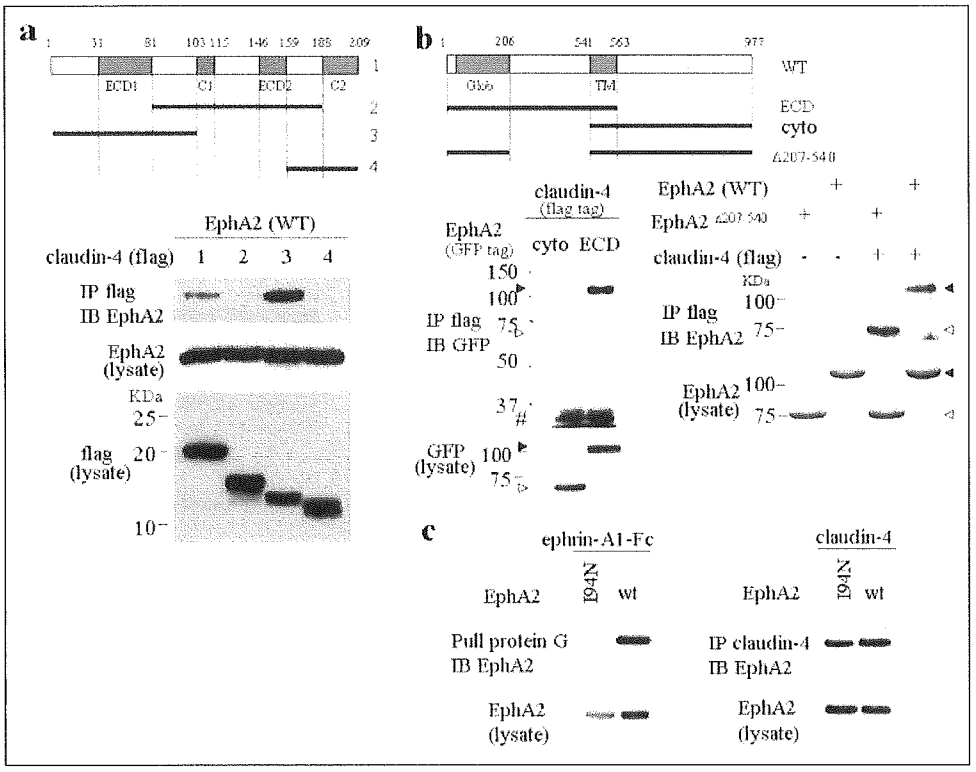

FIGURE 2. **The extracellular domains of EphA2 and claudin-4 are required for their association.** *a*, the amino-terminal region of claudin-4 binds to EphA2. *Upper panel*, schematic diagram of wild type and truncated claudin-4 cDNA constructs. *ECD1* and *ECD2*, the first and second extracellular domains; *C1* and *C2*, the first and second cytoplasmic domains. *Middle* and *lower panels*, COS1 cells were transiently transfected with plasmids encoding EphA2 and FLAG-tagged wild type or truncated claudin-4 constructs. The numbers above the lanes correspond to those in the diagram. FLAG-tagged claudin constructs were immunoprecipitated (*IP*) from cell lysates, and coprecipitated EphA2 was detected by immunoblotting (*IB*) with anti-EphA2 (*middle panel*). The expression of each construct in the cell lysates was confirmed by immunoblotting (*lower panels*). *b*, the amino-terminal region of EphA2 (amino acids 1–206) binds to claudin-4. *Upper panel*, schematic diagram of wild type and truncated EphA2 constructs. *Glob*, globular domain; *TM*, transmembrane domain. *Middle* and *lower left* and *right panels*, COS1 cells were transiently transfected with plasmids encoding FLAG-tagged wild type claudin-4 and truncated EphA2 constructs as indicated above the lanes. FLAG-tagged wild type claudin-4 was immunoprecipitated (*IP*) from cell lysates, and coprecipitated EphA2 constructs were detected by immunoblotting (*IB*) with the indicated antibodies. *Cyto*, EphA2 construct containing the cytoplasmic domain; *ECD*, EphA2 construct containing the extracellular domain. *Middle left panel*, *arrowheads* indicate ECD (*filled*) and Cyto (*open*) EphA2 constructs. *Middle right panel*, *arrowheads* indicate WT (*filled*) and Δ207–540 (*open*) EphA2 constructs. *Lower left* and *lower right panels*, the expression of each construct in the cell lysates was confirmed by immunoblotting. *Sharp sign* indicates IgG light chain. *c*, EphA2^{I94N} binds to claudin-4, but not to ephrin-A1. *Left panel*, COS1 cells were transiently transfected with plasmids encoding wild type (*wt*) or the I94N mutant of EphA2. The transfected cells were incubated with ephrin-A1-Fc (4 μg/ml) for 5 min and then lysed. The lysates were incubated with protein G-Sepharose to precipitate ephrin-A1-Fc, and coprecipitated EphA2 was detected by immunoblotting (*IB*). *Right panel*, COS1 cells were transiently transfected with claudin-4 and wild type (*wt*) or the I94N mutant of EphA2. Claudin-4 was immunoprecipitated (*IP*) from cell lysates, and coprecipitated EphA2 was detected by immunoblotting (*IB*).

FITC-dextran in the lower wells was determined using Beacon 2000 (Takara) with an excitation wavelength of 490 nm and detection of emissions at 530 nm.

RESULTS

Claudin Interacts with the Extracellular Domain of EphA2—Physical association between EphA2 and claudin-4 was first detected in COS1 cells transiently expressing both EphA2 and claudin-4. In these cells, EphA2 coprecipitated with claudin-4 immunoprecipitated with claudin-4-specific antibodies (Fig. 1*a*, *left panel*). Formation of an EphA2-claudin-4 complex was confirmed by immunoprecipitation using EphA2-specific antibodies (Fig. 1*a*, *right panel*). Endogenous EphA2 also coprecipitated with endogenous claudin-4 in extracts of the HT29 colon cancer cell line (Fig. 1*b*). Thus, endogenous EphA2 and claudin-4 physically interact in HT29 colon cancer cells.

Stimulation of EphA2 with ephrin-A1-Fc induces formation of membrane patches through the clustering of receptors (30–32). We examined changes in the localization of claudin-4 after stimulation of EphA2 with ephrin-A1-Fc. For efficient binding of the Fc fusion protein to the receptors, cells were plated at low density. In unstimulated HT29 cells, claudin-4 is diffusely expressed both on the cell membrane and in the cytoplasm (Fig. 1*c*, *left row*). Several minutes after exposure to ephrin-A1-Fc, claudin-4 redistributed as fine patches in the membrane that overlapped EphA2/ephrin-A1-Fc complexes (Fig. 1*c*, *middle row*). At 1 h after stimulation, partial colocalization of claudin-4 with EphA2/ephrin-A1-Fc was clearly observed as patchy complexes in the cytoplasm (Fig. 1*c*, *right row*). The dynamic colocalization of EphA2 and claudin-4 further indicates physiological association of these two molecules.

Next, a series of mutants of claudin-4 were generated to determine the region required for interaction with EphA2 (Fig. 2*a*). Among the mutants of claudin-4, the one containing the amino-terminal region including the first extracellular domain (ECD) tightly bound to EphA2 (Fig. 2*a*). Next, several mutants of EphA2 were utilized to determine the region involved in the interaction with claudin-4 (Fig. 2*b*). The extracellular domain, but not the cytoplasmic domain of EphA2, associates with claudin-4 (Fig. 2*b*, *left panel*). The amino-terminal region of EphA2 (amino acids 28–206) binds to its ligand, ephrin-A1 (33). Claudin-4 binds to EphA2-(Δ207–540), which contains the core region necessary for the interaction with its cognate ligand, ephrin-A1 (Fig. 2*b*, *right panel*). On the other hand, a specific EphA2 mutation, I94N, which was incidentally found to impair binding with ephrin-A1[3] (Fig. 2*c*, *left panel*), did not significantly affect EphA2 binding to claudin-4 (Fig. 2*c*,

[3] M. Tanaka and R. Sakai, unpublished data.

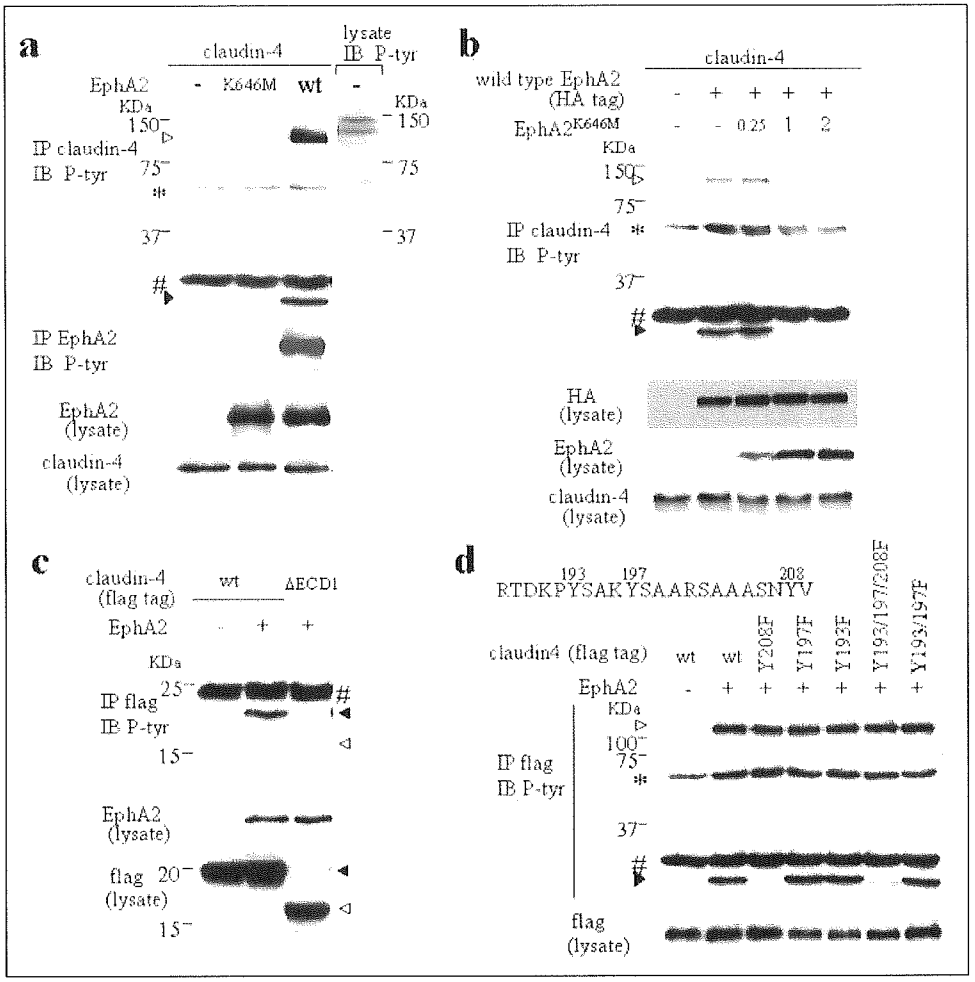

FIGURE 3. **Claudin-4 is tyrosine phosphorylated by the interaction with EphA2.** *a*, COS1 cells were transiently transfected with claudin-4 and wild type (*wt*) or a kinase-inactive mutant (*K646M*) of EphA2. *Upper panel*, claudin-4 was immunoprecipitated (*IP*) from cell lysates and subjected to immunoblotting with anti-phosphotyrosine (4G10). *Arrowheads* indicate tyrosine-phosphorylated EphA2 (*open*) and tyrosine-phosphorylated claudin-4 (*filled*). *Asterisk* and *sharp sign* indicate IgG heavy and light chains, respectively, which are not detected in the lysate of untransfected COS1 cells. *Middle panel*, EphA2 was immunoprecipitated (*IP*) from the cell lysates, and tyrosine phosphorylation of EphA2 was detected by immunoblotting (*IB*) with 4G10. *Bottom two panels*, EphA2 and claudin-4 detected in the lysate prior to immunoprecipitation. *b*, the kinase-inactive mutant of EphA2 competitively blocked the phosphorylation of claudin-4 by wild type EphA2. COS1 cells were transiently transfected with claudin-4 and hemagglutinin-tagged wild type EphA2 together with increasing amounts of kinase-inactive EphA2^{K646M} as indicated above the lanes. Assays were performed as in *panel a*. The expression level of wild type EphA2 (shown as immunoblotting with anti-hemagglutinin, *bottom panel*) was the same in each lysate. *Arrowheads* indicate tyrosine-phosphorylated EphA2 (*open*) and claudin-4 (*filled*). *Asterisk* and *sharp sign* indicate IgG heavy and light chains, respectively. *c*, claudin-4 lacking the binding region to EphA2 was not phosphorylated. COS1 cells were transiently transfected with wild type EphA2 and FLAG-tagged wild type claudin-4 or a mutant lacking the first extracellular domain of claudin-4 (Δ*ECD1*) as indicated above the lanes. *Upper panel*, claudin-4 was immunoprecipitated (*IP*) with anti-FLAG from cell lysates, and tyrosine-phosphorylated claudin-4 was detected by immunoblotting (*IB*) with anti-phosphotyrosine (4G10). *Arrowheads* indicate wild type (*filled*) and ΔECD1 claudin-4 (*open*). *Sharp sign* indicates IgG light chain. *Lower panels*, EphA2 and FLAG-tagged claudin-4 detected in the lysate prior to immunoprecipitation. *d*, EphA2 phosphorylates claudin-4 at Tyr-208. The amino acid sequence of the carboxyl tail of human claudin-4 is shown at the top with the tyrosine residues numbered. COS1 cells were transiently transfected with EphA2 together with FLAG-tagged wild type (*wt*) claudin-4 or claudin-4 with mutations at the indicated tyrosine residues. Assays were performed as in *panel c*. *Upper panel*, *arrowheads* indicate phosphorylated EphA2 (*open*) and claudin-4 (*filled*). *Asterisk* and *sharp sign* indicate IgG heavy and light chains, respectively. *Lower panel*, FLAG-tagged claudin-4 detected in the lysate prior to immunoprecipitation.

right panel). These data demonstrated that ephrin-A1 and claudin-4 both bind to the amino-terminal region of EphA2 (amino acids 1–206), but in different manners.

Claudin-4 Is Phosphorylated in the Cytoplasmic Tail upon Interaction with EphA2—EphA2 is known to exhibit ligand-independent activation by homophilic dimer formation when overexpressed in COS1 cells. Claudin-4 was clearly phosphorylated on tyrosine residue when coexpressed with wild type EphA2, but not when coexpressed with EphA2^{K646M}, a kinase-inactive EphA2 mutant (Fig. 3*a*). Moreover, EphA2^{K646M} blocked tyrosine phosphorylation of claudin-4 induced by wild type EphA2 in a dose-dependent manner (Fig. 3*b*). It was also observed that the claudin-4 mutant that lacks the EphA2-binding site (amino acids 81–209, claudin-4 ΔECD1) was not phosphorylated (Fig. 3*c*). These results indicate that association of EphA2 with claudin-4 and EphA2 kinase activity is required for phosphorylation of claudin-4.

Claudin-4 has three tyrosine residues in the second (carboxyl-terminal) cytoplasmic domain, but there is no tyrosine in the first (amino-terminal) cytoplasmic domain. Among the three tyrosine residues in the second cytoplasmic domain, the one located at the carboxyl terminus is well conserved in most claudin families (22). EphA2-induced phosphorylation of claudin-4 was completely abolished when the tyrosine at the carboxyl terminus was replaced by phenylalanine (claudin-4^{Y208F}), whereas substitution of other tyrosine residues did not affect the phosphorylation level of claudin-4 (Fig. 3*d*).

It was next determined whether cell-cell contact stimulates tyrosine phosphorylation of claudin-4 by physiological activation of EphA2. HT29 cells were used because they express the ephrin-A1 ligand, which can activate EphA2 upon cell-cell adhesion (34). In HT29 cells, both EphA2 and claudin-4 were highly phosphorylated on tyrosine residues when the cells were plated at high density, whereas their phosphoryla-

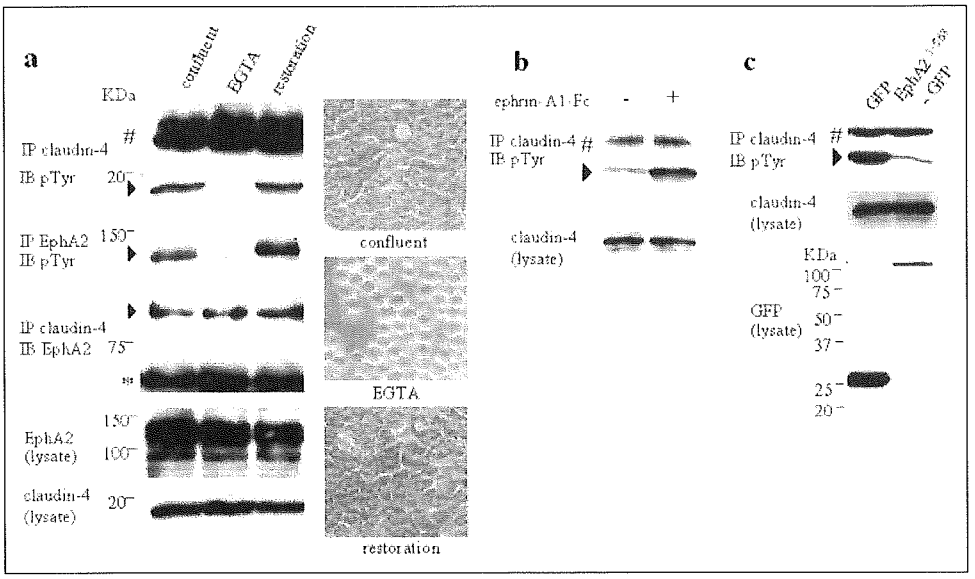

FIGURE 4. **Tyrosine phosphorylation of claudin-4 is induced by cell-cell contact.** *a*, HT29 cells were grown until confluent. The cells were either left untreated (*confluent*) or incubated in 2 mM EGTA in Hanks' balanced salt solution until cell-cell contacts were abolished but the cells remained attached to the plate (*EGTA*). EGTA was removed, and the cells were incubated in normal cell culture medium for 4 h (*restoration*). The cells were lysed at each time point and subjected to immunoprecipitation (*IP*) with anti-claudin-4 or anti-EphA2. Tyrosine-phosphorylated claudin-4 (*left column, top panel*) and tyrosine-phosphorylated EphA2 (*left column, second panel*) were detected by immunoblotting (*IB*) with anti-phosphotyrosine (4G10). EphA2 that coprecipitated with claudin-4 was detected by immunoblotting with anti-EphA2 (*left column, third panel*). Tyrosine-phosphorylated claudin-4, tryosine-phosphorylated EphA2, and coprecipitated EphA2 are indicated by *arrowheads*. *Sharp sign* and *asterisk* indicate IgG light and heavy chains, respectively. EphA2 and claudin-4 detected in the lysate prior to immunoprecipitation are shown in the *lower panels*. The appearance of the cells at each time point is shown in the *right panels*. *b*, HT29 cells plated at low cell density were treated with ephrin-A1-Fc for 10 min or left untreated (−). Claudin-4 was immunoprecipitated from each cell lysate, and tyrosine-phosphorylated claudin-4 was detected by immunoblotting (*IB*) with anti-phosphotyrosine (4G10). *Sharp sign* indicates IgG light chain. Claudin-4 detected in the lysate prior to immunoprecipitation is shown in the *lower panel*. *c*, confluent HT29 cells were infected with Ad-GFP or Ad-EphA2-(1–563)-GFP as indicated above the lanes. The infected cells were lysed, and the tyrosine phosphorylation of claudin-4 was examined as described in *panel b*. *Sharp sign* indicates IgG light chain. Claudin-4 and GFP and GFP-tagged EphA2 detected in the lysate prior to immunoprecipitation are shown in the *lower panels*.

tion level was very low when cell-cell interaction was disrupted by depletion of calcium in the medium (Fig. 4*a*). Treatment with nifedipine, a blocker of calcium channels, had no effect on the status of tyrosine phosphorylation of claudin-4 and EphA2 (data not shown), excluding the possibility that a decrease of intracellular calcium by EGTA affected the phosphorylation level of claudin. Treatment of HT29 cells with ephrin-A1-Fc enhanced phosphorylation of endogenous claudin-4 (Fig. 4*b*). Tyrosine phosphorylation of claudin-4 in HT29 cells was blocked by expression of EphA2-(1–563)-GFP, which does not contain the cytoplasmic region of EphA2 (Fig. 4*c*). These results suggest that claudin-4 is phosphorylated in HT29 cells when EphA2 is activated upon cell-cell interaction.

EphA2, however, remained associated with claudin-4 after disruption of cell-cell adhesion (Fig. 4*a*), even after the cells were dispersed as a single cell suspension through prolonged incubation with the calcium-chelating agent (data not shown). Therefore, the majority of association between EphA2 and claudin-4 occurred on the cell membrane of the same cells in *cis*, rather than on two different cells in *trans*.

Tyrosine Phosphorylation of Claudin-4 Attenuates Association with ZO-1—The carboxyl-terminal YV sequence of claudin associates with the PDZ domain of ZO-1 (22). We examined whether tyrosine phosphorylation of claudin-4 at the cytoplasmic tail affects interaction between claudin-4 and ZO-1. Non-phosphorylated and tyrosine-phosphorylated forms of recombinant GST-tagged claudin-4-(188–209), which contains the cytoplasmic tail, were purified using the TKX1 *E. coli* expression system (see "Experimental Procedures"). Non-phosphorylated claudin-4-(188–209) could effectively pull down the amino-terminal region of ZO-1 (N-ZO-1) expressed in COS1 cells. On the other hand, phosphorylated claudin-4 precipitated significantly lower amounts of N-ZO-1 (Fig. 5*a*, *lanes 1* and *2*). Because claudin-4-(188–209) contains three tyrosine residues (Fig. 3*d*), we also generated recombinant GST-claudin-4-(188–209)Y193/197F, in which two residual tyrosines were mutated, to confirm that phosphorylation of Tyr-208 of claudin-4 is responsible for attenuation of its binding ability with ZO-1. Non-phosphorylated wild type and the Y193/197F mutant of claudin-4-(188–209) equally coprecipitated ZO-1 (Fig. 5*a*, *lanes 1* and *3*), whereas phosphorylated claudin-4-(188–209)Y193/197F, in which only Tyr-208 was phosphorylated, did not effectively bind to ZO-1 (Fig. 5*a*, *lane 4*). Furthermore, neither claudin-4 lacking the carboxyl-terminal YV sequence nor GST alone bound to ZO-1 (Fig. 5*a*, *lanes 5* and *6*). Next, experiments were conducted to determine whether EphA2 activation leads to reduction of association between claudin-4 and ZO-1. The amount of claudin-4 coimmunoprecipitated with ZO-1 was reduced in EphA2-overexpressing COS1 cells (Fig. 5*b*). Association between claudin-4 and ZO-1 was also attenuated in MDCK cells expressing EphA2, and this association was further decreased by stimulation with ephrin-A1-Fc (Fig. 5*c*). From these results we conclude that EphA2 activation can reduce association of claudin-4 with ZO-1 by inducing phosphorylation of Tyr-208 of claudin-4 *in vivo*.

To examine the biological significance of EphA2-mediated attenuation of the binding affinity between claudin-4 and ZO-1, the change in localization of claudin-4 was monitored during the dynamic process of reestablishment of cell-cell adhesion. Wild type or the kinase-inactive mutant of EphA2 was expressed at high levels by adenovirus-mediated gene transfer in MDCK cells, which express endogenous claudin-4. When the cells were initially treated with calcium-chelating agent, ZO-1 and claudin-4 localization to cell-cell contact sites was completely abolished (data not shown). 30 min after replacing the calcium-free medium with normal growth medium (calcium switch), ZO-1 was found to relocalize to the cell-cell contact sites regardless of the presence of kinase-active or kinase-inactive EphA2 (Fig. 5*d*). On the other hand, in cells expressing kinase-dead EphA2, claudin-4 also relocalizes

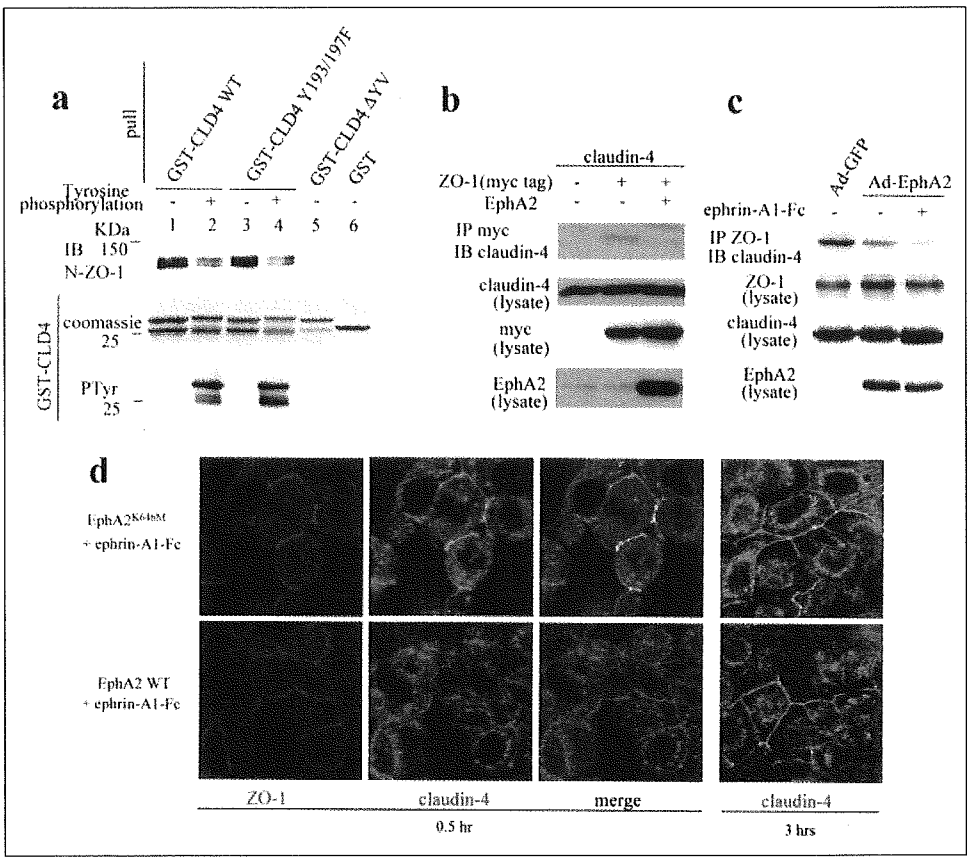

FIGURE 5. **Phosphorylation of claudin-4 at Tyr-208 inhibits interaction with ZO-1.** *a*, the second cytoplasmic domain of wild type (*WT*), the Y193/197F mutant, or the ΔYV mutant of claudin-4 was tagged with GST. The recombinant proteins were purified as either non-phosphorylated (−) or tyrosine phosphorylated (+) from TKX1-competent cells and incubated with lysate from N-ZO-1-transfected COS1 cells. The cell lysates were then incubated with protein G-Sepharose to precipitate claudin-4. *Upper panel*, coprecipitated N-ZO-1 was detected by immunoblotting (*IB*). *Middle panel*, purified GST fusion proteins added to the lysate are shown in a Coomassie Blue-stained gel. *Lower panel*, the tyrosine phosphorylation of recombinant GST-tagged claudin-4 was detected by immunoblotting with anti-phosphotyrosine (4G10). *b*, COS1 cells were transiently transfected with Myc-tagged ZO-1 and EphA2 as indicated above the lanes. ZO-1 was immunoprecipitated (*IP*) with anti-Myc antibody from cell lysates, and coprecipitated claudin-4 was detected by immunoblotting (*IB*). Claudin-4, ZO-1, and EphA2 detected in the lysates prior to immunoprecipitation are shown in the *lower panels*. *c*, MDCK cells infected with Ad-wild type EphA2 or control Ad-GFP were treated with EGTA. After removal of EGTA, the cells were incubated for 30 min in normal growth medium with (+) or without (−) ephrin-A1-Fc (4 μg/ml). ZO-1 was immunoprecipitated (*IP*) from the cell lysate, and coprecipitated claudin-4 was detected by immunoblotting (*IB*). ZO-1, claudin-4, and EphA2 detected in the lysates prior to immunoprecipitation are shown in the *lower panels*. *d*, MDCK cells infected with Ad-wild type EphA2 (*WT*) or Ad-EphA2^{K646M} were incubated with EGTA until cell-cell contacts were abolished. After removal of EGTA, the cells were incubated for 30 min or 3 h in normal growth medium with (+) or without (−) ephrin-A1-Fc (4 μg/ml) as indicated. The cells were then fixed and stained with anti-claudin-4 antibody or anti-ZO-1 antibody. Representative fields are shown.

to cell-cell contact sites 30 min after calcium switch, but in cells expressing kinase-active EphA2, claudin-4 did not relocalize to these sites (Fig. 5*d*). However, 3 h after calcium switch claudin-4 had relocalized to cell-cell contact sites in cells expressing kinase-active EphA2 (Fig. 5*d*). These results suggest that EphA2 causes a delay in reassembly of claudin-4 to tight junctions but has no effect on ZO-1.

EphA2 Affects Paracellular Permeability of Normal Epithelial Cells Depending on Its Kinase Activity—To examine the biological effect of the interaction of EphA2 with claudin-4 on tight junctions, paracellular permeability was measured using low molecular size dextran in MDCK epithelial cells. The amount of the dextran flux through a monolayer of confluent MDCK cells was almost undetectable even when EphA2 was overexpressed (data not shown). Therefore, we decided to examine the effect of EphA2 on reestablishment of the paracellular barrier after calcium switch. Overexpression of EphA2 effectively inhibited the prompt decrease of paracellular permeability through an MDCK monolayer after calcium switch, and this delay was further enhanced when cells were stimulated by ephrin-A1-Fc (Fig. 6*a*). On the other hand, kinase-inactive EphA2 did not affect paracellular permeability (Fig. 6*a*), indicating that the kinase activity of EphA2 affects permeability. In this experiment, the phosphorylation level of claudin-4 3 h after calcium switch had decreased to approximately the same level as in the confluent untreated cells (Fig. 6*b*, compare *lanes* 2 and 4). The paracellular flux of large molecular sized dextran (M_r 2,000) was below detectable levels at all time points shown in Fig. 6*a* (data not shown), indicating no massive destruction of junctional complexes had occurred in our experiment.

DISCUSSION

This is the first report showing tyrosine phosphorylation of claudin in relationship with its biological function. EphA2 induced the specific phosphorylation of Tyr-208 in the cytoplasmic tail of claudin-4 in COS1 cells, and endogenous claudin-4 was phosphorylated in response to EphA2 activation in HT29 cells. Both the kinase activity of EphA2 and association between EphA2 and claudin-4 are required for phosphorylation of claudin-4. Considering that EphA2 and claudin-4 associate on the same cell surface in *cis*, claudin-4 is most probably a direct substrate of EphA2. Our results indicate that activation of EphA2 by its ligand decreases integration of claudin-4 into tight junctions and enhances paracellular permeability.

Tyrosine phosphorylation of claudin-4 in its carboxyl-terminal tail inhibits binding to ZO-1. It is also reported that phosphorylation of the carboxyl-terminal tail of occludin by c-Src also attenuated its association with ZO-1, ZO-2, and ZO-3 *in vitro* (36). Thus, tyrosine phospho-

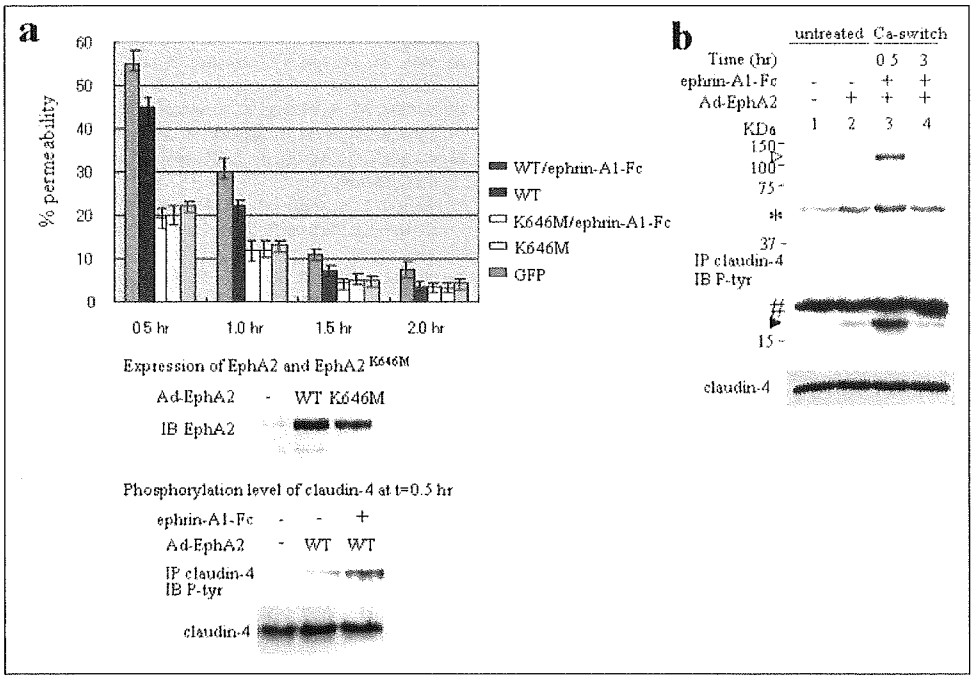

FIGURE 6. **EphA2 affects paracellular permeability and reassembly of claudin-4.** *a*, MDCK cells were grown until confluent in Transwell chambers. The cells were then infected with Ad-wild type EphA2 (*WT*), Ad-EphA2^{K646M} (*K646M*), or Ad-GFP. Two days later, the cells were treated with EGTA to disrupt cell-cell contacts, and then the EGTA was removed and replaced with normal growth medium (calcium switch). After the calcium switch, the cells were incubated in normal growth medium with (+) or without (−) ephrin-A1-Fc (4 μg/ml) for the indicated times. FITC-dextran was then added to the upper wells and the cells incubated for a further 30 min. After 30 min, the fluorescence of FITC-dextran in the lower wells was determined. The results are presented in terms of the % fluorescence in the lower wells when FITC-dextran was added to cell monolayers just after EGTA treatment. Each *bar* represents the mean value ± S.D. of three independent experiments. The expression of wild type EphA2 and EphA2^{K646M} is shown in the *middle panel*. The phosphorylation levels of claudin-4 in wild type EphA2-expressing cells with or without ephrin-A1-Fc 30 min after the calcium switch is shown in the *bottom panel*. *b*, confluent MDCK cells infected with Ad-wild type EphA2 (*lanes 2–4*) or not infected (*lane 1*) were either left untreated (*lanes 1* and *2*) or subjected to calcium switch as in *panel a* (*lanes 3* and *4*). After the calcium switch, the cells were incubated in normal growth medium containing ephrin-A1-Fc (4 μg/ml) for 30 min (*lane 3*) or 3 h (*lane 4*). The cells were then lysed, and claudin-4 was immunoprecipitated (*IP*) from the lysate. *Upper panel*, tyrosine-phosphorylated EphA2 and claudin-4 were detected by immunoblotting (*IB*) with anti-phosphotyrosine (4G10). *Arrowheads* indicate coprecipitated EphA2 phosphorylated on tyrosine (*open*) and immunoprecipitated claudin-4 phosphorylated on tyrosine (*filled*). *Asterisk* and *sharp sign* indicates IgG heavy chain and light chain, respectively. *Lower panel*, claudin-4 detected in the lysate prior to immunoprecipitation.

rylation within the PDZ domain-binding site is able to regulate protein-protein interaction.

Our results suggest that activation of EphA2 affects integration of claudin-4 into the sites of cell-cell contacts after calcium switch, thereby attenuating the barrier function of tight junctions. Although the mechanism of assembly of claudins and ZO-1 into tight junctions is not fully understood, ZO-1, which is primarily localized to tight junctions (35), presumably fails to recruit phosphorylated claudin-4 due to loss of physical association. This conclusion is consistent with the finding that claudin-4, but not ZO-1, localization to cell contacts is decreased after activation of EphA2 (Fig. 5*d*).

The EphA2-dependent increase of paracellular permeability was evident only during the dynamic process of tight junction reorganization triggered by calcium switch. On the other hand, expression of EphA2 did not effectively disrupt tight junctions, and junctional permeability and claudin-4 localization to cellular contacts were ultimately restored after calcium switch in MDCK cells even when claudin-4 was phosphorylated (Fig. 6*b*). These results suggest that phosphorylation of claudin-4 may affect the reassembly of tight junctions but not the maintenance of established tight junctions. One possibility is that the phosphorylation level of claudin-4 in confluent MDCK cells was relatively low and can be functionally compensated for by other members of the claudin family or by some other molecule. We are currently screening cell lines in which claudin-4 is highly phosphorylated at tight junctions to test this hypothesis.

Because of limitations in the availability of specific antibodies, the specificity of association between each member of the Eph family and the claudin family is still uncertain. At least one other Eph family member, EphA4, is likely to be involved in this cross-talk, as claudin-4 was also tyrosine phosphorylated by coexpression with EphA4 in COS1 cells (data not shown). Also, the tyrosine residue located at the carboxyl terminus is conserved among at least 8 claudin family members, claudin-1–8. Therefore, other claudins also have the potential to be phosphorylated by Eph receptors. We are currently testing this hypothesis.

In tumors overexpressing EphA2, assembly of tight junctions may be negatively regulated via phosphorylation of claudin. This has the potential to affect the malignant phenotype of the carcinoma, such as loss of cell polarity. Moreover, in tumors overexpressing both EphA2 and claudin-4, like HT29 colon cancer cells, phosphorylation of claudin-4 might transduce signals distinct from tight junction function. We are currently attempting to identify other downstream targets of signaling through tyrosine phosphorylation of claudin-4 and determine their roles in the regulation of epithelial cells and cancer cells.

Acknowledgments—We thank Dr. S. Tsukita (Kyoto University) for providing the plasmids used in this study. We thank Dr. B. J. Mayer (University of Connecticut Health Center) and Dr. D. B. Alexander (Dept. of Molecular Toxicology, Nagoya City University) for critically reading this manuscript.

REFERENCES

1. Blits-Huizinga, C., Nelersa, C., Malhotra, A., and Liebl, D. (2004) *IUBMB Life* **56**, 257–265
2. Murai, K. K., and Pasquale, E. (2003) *J. Cell Sci.* **116**, 2823–2832
3. Kullander, K., and Klein, R. (2002) *Nat. Rev. Mol. Cell. Biol.* **3**, 475–486
4. Poliakov, A., Cotrina, M., and Wilkinson, D. G. (2004) *Dev. Cell* **7**, 465–480

5. Huot, J. (2004) *Prog. Neuropsychopharmacol. Biol. Psychiatry* **28,** 813–818
6. Hinck, L. (2004) *Dev. Cell* **7,** 783–793
7. Mann, F., Harris, W. A., and Holt, C. E. (2004) *Int. J. Dev. Biol.* **48,** 957–964
8. Bolz, J., Uziel, D., Muhlfriedel, S., Gullmar, A., Peuckert, C., Zarbalis, K., Wurst, W., Torii, M., and Levitt, P. (2004) *J. Neurobiol.* **59,** 82–94
9. Klein, R. (2004) *Curr. Opin. Cell Biol.* **16,** 580–589
10. Brantley-Sieders, D., Parker, M., and Chen, J. (2004) *Curr. Pharm. Des.* **10,** 3431–3442
11. Surawska, H., Ma, P. C., and Salgia, R. (2004) *Cytokine Growth Factor Rev.* **15,** 419–433
12. Kinch, M. S., and Carles-Kinch, K. (2003) *Clin. Exp. Metastasis* **20,** 59–68
13. Brantley-Sieders, D. M., and Chen, J. (2004) *Angiogenesis* **7,** 17–28
14. Cheng, N., Brantley, D. M., and Chen, J. (2002) *Cytokine Growth Factor Rev.* **13,** 75–85
15. Kataoka, H., Igarashi, H., Kanamori, M., Ihara, M., Wang, J. D., Wang, Y. J., Li, Z. Y., Shimamura, T., Kobayashi, T., Maruyama, K., Nakamura, T., Arai, H., Kajimura, M., Hanai, H., Tanaka, M., and Sugimura, H. (2004) *Cancer Sci.* **95,** 136–141
16. Orsulic, S., and Kemler, R. (2000) *J. Cell Sci.* **113,** 1793–1802
17. Zantek, N. D., Azimi, M., Fedor-Chaiken, M., Wang, B., Brackenbury, R., and Kinch, M. S. (1999) *Cell Growth Differ.* **10,** 629–638
18. Jones T. L., Chong, L. D., Kim, J., Xu, R. H., Kung, H. F., and Daar, I. O. (1998) *Proc. Natl. Acad. Sci. U. S. A.* **95,** 576–581
19. Winning, R. S., Scales, J. B., and Sargent, T. D. (1996) *Dev. Biol.* **179,** 309–319
20. Morita, K., Furuse, M., Fujimoto, K., and Tsukita, S. (1999) *Proc. Natl. Acad. Sci. U. S. A.* **96,** 511–516
21. Tsukita, S., Furuse, M., and Itoh, M. (2001) *Nat. Rev. Mol. Cell. Biol.* **2,** 285–293
22. Itoh, M., Furuse, M., Morita, K., Kubota, K., Saitou, M., and Tsukita, S. (1999) *J. Cell Biol.* **147,** 1351–1363
23. Hamazaki, Y., Itoh, M., Sasaki, H., Furuse, M., and Tsukita, S. (2002) *J. Biol. Chem.* **277,** 455–461
24. Roh, M. H., Liu, C., Laurinec, S., and Margolis, B. (2002) *J. Biol. Chem.* **277,** 27501–27509
25. Aldred, M. A., Huang, Y., Livanarachchi, S., Pellegata, N. S., Gimm, O., Jhiang, S., Davuluri, R. V., de la Chapelle, A., and Eng, C. (2004) *J. Clin. Oncol.* **22,** 3531–3539
26. Nicols, L. S., Ashfag, R., and Lacobuzio-Donahue, C. A. (2004). *Am. J. Clin. Pathol.* **121,** 226–230
27. Rangel, L. B., Agarwal, R., D'Souza, T., Pizer, E. S., Alo, P. L., Lancaster, W. D., Gregoire, L., Schwartz, D. R., Cho, K. R., and Morin, P. J. (2003) *Clin. Cancer Res.* **9,** 2567–2575
28. Wang, Y., Ota, S., Kataoka, H., Kanamori, M., Li, Z., Band, H., Tanaka, M., and Sugimura, H. (2002) *Biochem. Biophys. Res. Commun.* **296,** 214–220
29. Tanaka, M., Ohashi, R., Nakamura, R., Shinmura, K., Kamo, T., Sakai, R., and Sugimura, H. (2004) *EMBO J.* **23,** 1075–1088
30. Palmer, A., Zimmer, M., Erdmann, K. S., Eulenburg, V., Porthin, A., Heumann, R., Deutsch, U., and Klein, R. (2002) *Mol. Cell.* **9,** 725–737
31. Cowan, C. A., and Henkemeyer, M. (2001) *Nature* **413,** 174–179
32. Cowan, C. A., and Henkemeyer, M. (2002) *Trends Cell Biol.* **12,** 339–346
33. Himanen, J. P., Rajashankar, K. R., Lackmann, M., Cowan, C. A., Henkemeyer, M., and Nikolov, D. B. (2001) *Nature* **414,** 933–938
34. Potla, L., Boghaert, E. R., Armellino, D., Frost, P., and Damle, N. K. (2002) *Cancer Lett.* **175,** 187–195
35. Rothen-Rutishauser, B., Riesen, F. K., Braun, A., Gunthert, M., and Wunderli-Allenspach, H. (2002) *J. Membr. Biol.* **188,** 151–162
36. Kale, G., Naren, A., Sheth, P., and Rao, R. K. (2003) *Biochem. Biophys. Res. Commun.* **302,** 324–329

THE JOURNAL OF BIOLOGICAL CHEMISTRY
Vol. 280, No. 12, Issue of March 25, pp. 11467–11474, 2005
Printed in U.S.A.

The Fission Yeast Protein Ker1p Is an Ortholog of RNA Polymerase I Subunit A14 in *Saccharomyces cerevisiae* and Is Required for Stable Association of Rrn3p and RPA21 in RNA Polymerase I*

Received for publication, September 29, 2004, and in revised form, January 10, 2005
Published, JBC Papers in Press, January 12, 2005, DOI 10.1074/jbc.M411150200

Yukiko Imazawa‡§¶, Koji Hisatake‡, Hiroshi Mitsuzawa‖, Masahito Matsumoto‡, Tohru Tsukui‡¶, Kaori Nakagawa‡§, Tomoyoshi Nakadai‡, Miho Shimada‡, Akira Ishihama, and Yasuhisa Nogi‡ ‡‡**

*From the ‡Department of Molecular Biology, Saitama Medical School, 38 Morohongo, Moroyama, Iruma-gun, Saitama 350-0495, Japan, the §Japan Science and Technology Corporation Center, Kawaguchi, Saitama 332-0012, Japan, the ¶Research Center for Genomic Medicine, Saitama Medical School, Hidaka, Saitama 350-1241, Japan, the ‖Department of Molecular Genetics, National Institute of Genetics, Mishima, Shizuoka 411-8540, Japan, and the **Nippon Institute for Biological Science, Oume, Tokyo 198-0024, Japan*

A heterodimer formed by the A14 and A43 subunits of RNA polymerase (pol) I in *Saccharomyces cerevisiae* is proposed to correspond to the Rpb4/Rpb7 and C17/C25 heterodimers in pol II and pol III, respectively, and to play a role(s) in the recruitment of pol I to the promoter. However, the question of whether the A14/A43 heterodimer is conserved in eukaryotes other than *S. cerevisiae* remains unanswered, although both Rpb4/Rpb7 and C17/C25 are conserved from yeast to human. To address this question, we have isolated a *Schizosaccharomyces pombe* gene named *ker1*$^+$ using a yeast two-hybrid system, including *rpa21*$^+$, which encodes an ortholog of A43, as bait. Although no homolog of A14 has previously been found in the *S. pombe* genome, functional characterization of Ker1p and alignment of Ker1p and A14 showed that Ker1p is an ortholog of A14. Disruption of *ker1*$^+$ resulted in temperature-sensitive growth, and the temperature-sensitive deficit of *ker1*Δ was suppressed by overexpression of either *rpa21*$^+$ or *rrn3*$^+$, which encodes the rDNA transcription factor Rrn3p, suggesting that Ker1p is involved in stabilizing the association of RPA21 and Rrn3p in pol I. We also found that Ker1p dissociated from pol I in post-log-phase cells, suggesting that Ker1p is involved in growth-dependent regulation of rDNA transcription.

There are three distinct types of eukaryotic nuclear RNA polymerases: RNA polymerase (pol)[1] I, pol II, and pol III. Among eukaryotic organisms, the structure and function of RNA polymerases in *Saccharomyces cerevisiae* have been studied fairly extensively (1–4). *S. cerevisiae* pol I consists of 14 subunits. The core structure contains 10 subunits (A190, A135, AC40, AC19, Rpb5, Rpb6, Rpb8, Rpb10, Rpb12, and A12.2) and is believed to be sufficient for nonspecific transcription, but not for accurate initiation of transcription (5). In fact, pol I requires four specific subunits (A49, A43, A34.5, and A14) for specific transcription of rDNA. A43 is also essential for cell growth (6), whereas A49 (7), A34.5 (8), and A14 (9) are dispensable.

Much attention has recently been focused on the A14 and A43 subunits in view of the structural and functional conservation of these two subunits in eukaryotes. A43 is conserved in a variety of eukaryotes (10) and shows amino acid sequence similarity to Rpb7 (a specific subunit of pol II), C25 (a specific subunit of pol III), and RpoE (a subunit of archaeal RNA polymerases) across multiple RNA polymerases (11). Furthermore, A43 forms a heterodimer with A14 that is similar to the Rpb4/Rpb7 (11, 12), C17/C25 (13), and RpoF/RpoE (14) heterodimers in pol II, pol III, and archaeal RNA polymerases, respectively. It should be noted that Rpb4, C17, and RpoF have mutual sequence similarity and are grouped into a gene family, but no obvious homolog of A14 has been found in available data bases. A14 and Rpb4 are required for the stable assembly of A43 and Rpb7, respectively, in their respective RNA polymerases, suggesting a functional similarity of A14 to Rpb4 (5, 11, 15, 16). The position of A14/A43 in the three-dimensional structure of pol I has been deduced to be similar to that of Rpb4/Rpb7, forming an upstream interface with the C-terminal domain of Rpb1 to interact with transcription factor IIB for pol II recruitment to the pol II promoter (4) and, furthermore, playing a role in the processing of the nascent RNA transcript (17). Consistent with the proposed position in pol I, A14/A43 also interacts with an rDNA-specific transcription factor (Rrn3p) for pol I recruitment to the rDNA promoter (10) and is able to bind to single-stranded RNA (18). Interestingly, C17/C25 in pol III is also reported to interact with transcription factor IIIB, which recruits pol III to the pol III promoter (19).

The mechanism of the down-regulation of rDNA transcription (20–24) is now believed to be as follows. Only a small fraction of pol I associated with Rrn3p is able to recognize the components of the preinitiation complex, resulting in pol I recruitment to the rDNA promoter (25–28). A43 in pol I is responsible for associating with Rrn3p (10), and the association of A43 with Rrn3p is inhibited in post-log-phase cells (including nutrient-starved or growth-arrested cells) (24, 26), resulting in a drastic decrease in pol I recruitment to the promoter (29).

* This work was supported by the Core Research for Evolutional Science and Technology of the Japan Science and Technology Corporation, by a Human Frontier Science Program Organization grant, and by a grant for the promotion of the advancement of education and research in graduate schools from the Ministry of Education, Culture, Sports, Science, and Technology of Japan. The costs of publication of this article were defrayed in part by the payment of page charges. This article must therefore be hereby marked "*advertisement*" in accordance with 18 U.S.C. Section 1734 solely to indicate this fact.

The nucleotide sequence(s) reported in this paper has been submitted to the DDBJ/GenBank™/EBI Data Bank with accession number(s) AB07137.

‡‡ To whom correspondence should be addressed. Tel.: 81-492-76-1490; Fax: 81-492-94-9751; E-mail: yasunogi@saitama-med.ac.jp.

[1] The abbreviations used are: pol, RNA polymerase; 3-AT, 3-amino-1,2,4-triazole; HA, hemagglutinin; Gal4DB, Gal4 DNA-binding domain; CMV, cytomegalovirus; GFP, green fluorescent protein; DAPI, 4′,6-diamidino-2-phenylindole.

TABLE I
Yeast strains and plasmids

Strains and plasmids	Description
Strains	
S. pombe	
JY742	*h⁺ ade6-M216 ura4-D18 leu1*
JY745	*hj⁻ ade6-M210 ura4-D18 leu1*
IZ2	Derivative of JY742 expressing RPA140 tagged with His_6-FLAG (42)
YI28	Derivative of IZ2 expressing *ker1⁺*-HA_3
YI29	Diploid (crossing JY742 with JY745) carrying *ker1Δ::ura4⁺/ker1⁺*
YI30	*h⁻ ker1Δ::ura4⁺ ade6 ura4-D18 leu1*
S. cerevisiae	
Y190	*MAT***a** *ade2-101 ura3-52 his3-Δ200 lys2-801 trp1-901 leu2-3,112 gal4Δ gal80Δ LYS2::GAL1-HIS3 URA3::GAL1-lacZ*
Plasmids	
pKI45	Derivative of KS(+) cloned with full-length cDNA of *rpa21⁺* between XhoI and EcoRI sites
pYI77	Derivative of pAS2-1 expressing Gal4DB-RPA21, *TRP1*, 2μm
pKS406	Derivative of pSGA (47) expressing GFP fusion proteins under control of *nmt1* promoter, *ars1*, *LEU2*
pYI193	Derivative of pKS406 expressing GFP-Ker1p
pYI200	Derivative of pKS406 expressing GFP-fibrillarin
pYN1235	Derivative of pGEM3ZpBR322ura4⁺pBR322 with BamHI site introduced into HindIII site (55)
pYN1237	Derivative of KS(+); HA_3-TAG sequence (triple-HA epitope tagged with TAG) inserted between SmaI and SpeI sites; 2.5-kb BamHI-BamHI *ura4⁺* fragment excised from pYN1235 inserted at BglII site created downstream of HA_3-TAG sequence
pAUR224	Expression vector under control of CMV promoter, *aur1ʳ*, *ars1*
pYI195	Derivative of pAUR224 expressing full-length Ker1p under control of CMV promoter
pYI176	Derivative of pYN1237 carrying 1.0-kb fragment of 5′-flanking and coding sequence of Ker1p-HA_3, *ura4⁺*, and 1.0-kb fragment of 3′-flanking sequence of *ker1⁺*
pGK100	Derivative of pDB248 carrying *nuc1⁺/rpa190⁺* (37)
pYI185	Derivative of KS(+) carrying 0.88-kb fragment of 5′-flanking region of *ker1⁺* between XhoI and BamHI sites and 1.0-kb fragment of 3′-flanking region of *ker1⁺* between NotI and SacI sites
pYI186	Derivative of pYI185 with *ura4⁺* inserted at BamHI site
pREP41	Expression vector under control of modified *nmt1* promoter, *LEU2*, *ars1* (56)
pREP81	Expression vector under control of modified *nmt1* promoter, *LEU2*, *ars1* (56)
pYI40	Derivative of pREP81 with NdeI site converted to BglII site (41)
pYI82	Derivative of pYI40 expressing *rpa21⁺* cDNA under control of weak *nmt1* promoter (41)
pKI27	Derivative of pREP81 expressing full-length *rrn3⁺* under control of *nmt1* promoter
pYI210	Derivative of pYI40 expressing full-length *ker1⁺* under control of *nmt1* promoter

Thus, the molecular function of A43 and Rrn3p deserves further study to resolve long-standing questions regarding growth-dependent transcription of rDNA (30).

It is firmly established that all 12 and all 17 subunits of *S. cerevisiae* pol II and pol III, respectively, are conserved in human pol II and pol III (31, 32). However, it is not clear whether all 14 subunits identified in *S. cerevisiae* pol I are conserved in other eukaryotes (33, 34). To gain further insight into the structure and function of pol I, we have been studying pol I of *Schizosaccharomyces pombe*, which is only distantly related to *S. cerevisiae*, but is amenable to genetic analysis (35). To date, it is known that *S. pombe* pol I consists of at least 12 subunits. The two largest, RPA190 and RPA140, are homologous to A190 and A135, respectively (36, 37). The two smaller subunits, RPA42 and RPA17, correspond to AC40 and AC19, respectively (38, 39). Five common subunits (Rpb5, Rpb6, Rpb8, Rpb10, and Rpb12) are shared by pol II and pol III (12), and SpRPA12 is a functional homolog of A12.2 (40). Thus, the 10-subunit core structure of pol I has been well conserved between the two yeasts through evolution. Moreover, the two specific subunits in *S. pombe*, RPA21 and RPA51, have been identified to be related to A43 and as a functional homolog of A49, respectively, suggesting that the pol I architecture in *S. pombe* is likely to be analogous to that in *S. cerevisiae* (41, 42).

In this study, we demonstrate that a newly isolated protein, Ker1p, is an ortholog of A14 and that the Ker1p/RPA21 heterodimer in *S. pombe* is the functional counterpart of A14/A43 in *S. cerevisiae*. We also show novel aspects of Ker1p that have not been previously observed in A14 and suggest that Ker1p is involved in growth-dependent transcription of rDNA.

EXPERIMENTAL PROCEDURES

Media, Strains, and Genetic Techniques—The yeast plasmids and strains used are listed in Table I. Minimal medium with or without thiamine and supplemented with appropriate amino acids and yeast extract/dextrose medium were prepared to grow *S. pombe* cells as described previously (35). Yeast extract/peptone/dextrose medium and synthetic dextrose medium were prepared as described previously (43). Synthetic dextrose medium lacking tryptophan and leucine and synthetic dextrose medium containing 25 mM 3-amino-1,2,4-triazole (3-AT) were used. Minimal medium containing 0.1–0.4 μg/ml aureobasidin A was also used. Disruption of chromosomal *ker1⁺* was carried out as follows. Diploid cells (a cross between JY742 and JY745 cells) were transformed with the 4.5-kb XhoI-SacI linear fragment containing *ker1Δ::ura4⁺* from pYI186. To replace Ker1p with Ker1p-HA_3, a 5.0-kb XhoI-SacI fragment from pYI176 (see below) was transformed into strain IZ2, resulting in YI28.

Plasmids—For two-hybrid screening, Gal4DB-*rpa21⁺* (pYI77) was constructed as follows. 0.52-kb *rpa21⁺* cDNA was amplified by PCR using pKI45 containing a full-length 0.52-kb cDNA of *rpa21⁺* (41) as a template and cloned between the SmaI and XhoI sites of pAS2-1 (44) to fuse Gal4DB to RPA21 in-frame. To construct deletion derivatives of *rpa21⁺*, pKI45 was also used as template DNA for PCR amplification. pYI106 expresses RPA21 with the N-terminal 56 amino acids truncated fused to Gal4DB, whereas pYI105 expresses RPA21 with the C-terminal 60 amino acids truncated fused to Gal4DB. To replace chromosomal *ker1⁺* with *ker1⁺*-HA_3, a PCR-amplified 1317-bp XhoI-SmaI fragment of the 5′-untranslated region and open reading frame of *ker1⁺* and a 1017-bp NotI-SacI fragment of the 3′-flanking region of *ker1⁺* were cloned successively between the XhoI and SmaI sites and the NotI and SacI sites of pYN1237, generating pYI176. To express Ker1p under the control of the cytomegalovirus (CMV) promoter in *S. pombe*, full-length *ker1⁺* (441 bp) was amplified from JY742 DNA by PCR and cloned between the XhoI and BamHI sites of pAUR222 (TaKaRa), resulting in pYI195. To study the cellular localization of Ker1p, full-length *ker1⁺* was amplified from JY742 DNA, and the 441-bp fragment was cloned between the NotI and BamHI sites of pKS406 to express a GFP-Ker1p fusion protein, resulting in pYI193. A GFP-fibrillarin fusion construct was made using a 912-bp fragment of the *fib* gene encoding fibrillarin, which was amplified by PCR from JY742 DNA and cloned between the NotI and BamHI sites of pKS406, resulting in pYI200. To construct a disrupted *ker1Δ::ura4⁺* allele, we amplified the 880-bp 5′-untranslated sequence of *ker1⁺* flanked by the XhoI and BamHI sites and the 1.0-kb 3′-untranslated sequence of *ker1⁺* flanked by the NotI and SacI sites

from the JY742 genome. Each PCR product was cloned successively between the XhoI and BamHI sites and between the NotI and SacI sites of pBluescript II KS(+), resulting in pYI185. Then, the 2.5-kb BamHI-BamHI DNA fragment of *ura4*$^+$ obtained from pYN1235 was cloned into the BamHI site of the resulting plasmid, generating pYI186. To construct pKI27, full-length *rrn3*$^+$ was amplified by PCR from JY742 DNA and cloned between the SalI and SmaI sites of pREP81. To express *ker1*$^+$ under the control of the *nmt1* promoter, full-length *ker1*$^+$ was amplified by PCR from JY742 DNA and cloned between the SalI and BamHI sites of pYI40, generating pYI210. *Pfu* DNA polymerase was used for PCR, and DNA sequencing analysis was used to confirm the PCR product.

Two-hybrid Screening—pYI77 expressing a Gal4DB-RPA21 bait was transformed into the reporter strain Y190. Y190 carrying pYI77 was transformed with an *S. pombe* cDNA library fused to Gal4 activation domain in pGAD-GH (Clontech). The 3-AT-resistant and His$^+$ transformants were screened on synthetic dextrose medium plates without Trp and Leu and containing 25 mM 3-AT. *lacZ* activation was examined by a filter lifting assay (38).

Fluorescence Microscopy of GFP Fusion Proteins—To visualize the nuclear chromatin region, cells were stained with 4′,6-diamidino-2-phenylindole (DAPI) at 1 mg/ml. Fluorescent images were obtained with a Fujix HC-2500 CCD camera using a Zeiss Axioskop fluorescence microscope.

Immunoprecipitation—*S. pombe* cells were grown in yeast extract/dextrose medium and harvested in mid-log phase. Preparation of cell extracts and immunoprecipitation with anti-HA epitope monoclonal antibody 12CA5 (Roche Applied Science) and anti-RPA190 antibody were carried out as described by Mitsuzawa *et al.* (45). Immunoblotting was performed essentially as described previously (39) using polyclonal antibodies against RPA190, RPA140, RPA21, and Rpb1 (pol II) (41, 46).

Biochemical Fractionation of pol I—pol I was partially purified as described previously (46). Whole cell extract from strain YI28 was loaded onto a nickel-nitrilotriacetic acid-agarose column. The proteins eluted with 200 mM imidazole were loaded onto a DEAE-Sephadex A25 column and eluted with a 50–620 mM ammonium sulfate gradient. Fractions were examined by SDS-PAGE, followed by Western blotting using antibodies against RPA190, RPA21, and HA. (Ker1p was tagged with HA_3 in strain YI28.)

Phosphatase Treatment—Whole cell extract was prepared form strain YI28, and 1.6 mg of protein was immunoprecipitated with anti-RPA190 antibody (10 μl of antiserum) as described above. The precipitates were washed three times with 20 mM HEPES-KOH (pH 7.6), 150 mM potassium acetate, 20% glycerol, 0.1% Nonidet P-40, and 1 mM dithiothreitol and once with HM buffer (50 mM HEPES-KOH (pH 7.6) and 1 mM $MgCl_2$). The pellet was resuspended in 1 ml of HM buffer, divided into four aliquots, centrifuged again, resuspended with 100 μl of HM buffer, and incubated for 10 min at 30 °C. Calf intestine alkaline phosphatase (30 units, 1.5 μl; Roche Applied Science) was added to one tube and incubated for 20 min at 30 °C. The reaction was stopped by addition of SDS sample buffer and heating at 95 °C for 5 min. In controls, sodium pyrophosphate (final concentration of 5.4 mM) was added with or without alkaline phosphatase, and the sample was then treated as described above. No treatment was performed for the fourth sample. All samples were subjected to 8% SDS-PAGE, followed by immunoblot analysis with anti-HA antibody.

RESULTS

Identification of a Novel Protein (Ker1p) That Interacts with the RPA21 Subunit—To identify protein(s) that interact with RPA21, we generated a Gal4DB-RPA21 fusion construct in pAS2-1 (pYI77) and introduced it into the *S. cerevisiae* two-hybrid reporter strain Y190. Subsequently, we introduced an *S. pombe* cDNA library fused to the Gal4 activation domain into the Y190 strain carrying pYI77. We selected ~10^7 Leu$^+$ transformants and screened colonies showing 3-AT resistance and a *lacZ*-positive phenotype. In total, 27 transformants showing 3-AT resistance and the *lacZ*-positive phenotype were obtained, and the responsible plasmids carrying cDNA fused to the Gal4 activation domain were retrieved (data not shown). Nucleotide sequencing of the retrieved plasmids indicated that all of the cDNAs encoding the protein shown to interact with RPA21 were derived from the same gene; one group lacked the C-terminal 30 amino acids, and another retained the full-length gene, indicating that the C-terminal 30 amino acids are not required for interaction with RPA21 in the yeast two-hybrid method. The gene isolated by the two-hybrid system encodes a protein of 147 amino acids with a calculated molecular mass of 16,976 Da and a calculated pI of 6.25. The predicted protein is very hydrophilic and contains many charged amino acids: 21 lysine residues, 9 arginine residues, 24 glutamic acid residues, and 7 aspartic acid residues (see Fig. 7). Therefore, we have named this protein Ker1p (for lysine (K) and glutamic acid (E)-rich protein 1) and the gene encoding it *ker1*$^+$. No proteins homologous to Ker1p were observed in an initial data base search.

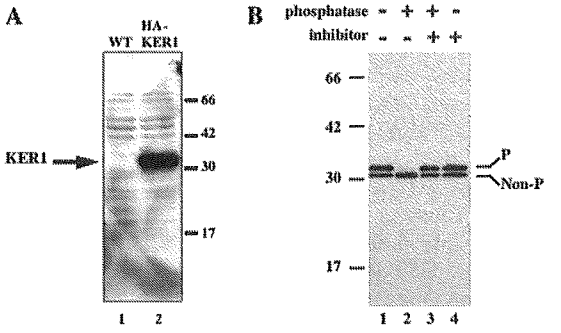

FIG. 1. **Ker1p can be phosphorylated.** *A*, apparent molecular mass of Ker1p. Extracts prepared from *S. pombe* cells of strains IZ2 (wild type (*WT*)) and YI28 expressing Ker1p-HA_3 (*HA-KER1*) were subjected to SDS-PAGE, followed by immunoblot analysis with monoclonal antibody 12CA5. In *lanes 1* and *2*, 40 μg of crude extract was loaded. *B*, Ker1p is a phosphorylated protein. Ker1p-HA_3 was immunoprecipitated from a whole cell extract of strain YI28 with monoclonal antibody 12CA5. The immunoprecipitates were treated as follows: no treatment (*lane 1*), alkaline phosphatase (*lane 2*), alkaline phosphatase and a phosphatase inhibitor (sodium pyrophosphate; *lane 3*), and the inhibitor alone (sodium pyrophosphate; *lane 4*). After treatment, samples were subjected to SDS-PAGE, followed by immunoblot analysis with monoclonal antibody 12CA5. Molecular mass standards (in kilodaltons) are indicated on the right in *A* and on the *left* in *B*. *P*, phosphorylated Ker1p; *Non-P*, non-phosphorylated Ker1p.

Apparent Molecular Mass of Ker1p-HA_3—To determine the apparent molecular mass of Ker1p, a YI28 strain expressing Ker1p-HA_3 was constructed. Whole cell extracts prepared from YI28 and the parental strain IZ2, in which Ker1p had not been tagged, were subjected to SDS-PAGE, followed by immunoblotting with anti-HA monoclonal antibody 12CA5. Fig. 1*A* shows that Ker1p-HA_3 was detected as a doublet of bands at 30 and 32 kDa, including a triple-HA sequence (4.3 kDa). Since the calculated molecular mass of Ker1p is ~17 kDa, it appears that Ker1p-HA_3 migrates abnormally on SDS-polyacrylamide gel, for unknown reasons.

Ker1p Is Phosphorylated—The predicted amino acid sequence of Ker1p suggested that it contains many consensus phosphorylation sites for protein kinase A (Ser^{14}), protein kinase C (Ser^{14}, Ser^{22}, and Ser^{94}), casein kinase I (Ser^{45}), casein kinase II (Ser^{41} and Thr^{89}), and glycogen synthase kinase I (Ser^{41}, Ser^{45}, Ser^{94}, and Thr^{89}) (see Fig. 7). We considered the possibility that Ker1p is phosphorylated and that both phosphorylated and non-phosphorylated forms were detected as doublet bands by immunoblotting in Fig. 1*A*. Therefore, Ker1p-HA_3 was first immunoprecipitated with anti-HA antibody, and the immunoprecipitates were then treated with alkaline phosphatase in the absence or presence of a phosphatase inhibitor. As shown in Fig. 1*B*, phosphatase treatment resulted in the appearance of only the faster moving 30-kDa band (*lane 2*). No treatment (*lane 1*), treatment with phosphatase and an inhibitor (*lane 3*), or treatment with the inhibitor only (*lane 4*) generated two bands of 30 and 32 kDa, similar to those observed in Fig. 1*A* (*lane 2*). Therefore, we conclude that the 30-kDa band represents non-phosphorylated Ker1p-HA_3 and that the 32-kDa band represents phosphorylated Ker1p-HA_3.

Ker1p Is Localized Predominantly in the Nucleolus—Because Ker1p interacts with RPA21 of pol I, which localizes specifically in the nucleolus, we examined whether Ker1p also localizes in the nucleolus using a GFP-Ker1p fusion protein. Fig. 2 (*A–C*) shows that GFP-Ker1p formed a dense, crescent-shaped structure that occupied one side of the nucleus and that the crescent-shaped region was not stained well by DAPI. The observed crescent-shaped structure with much reduced DNA staining is the most obvious characteristic of the yeast nucleolus (37, 47, 48). However, GFP-Ker1p was also observed in the DAPI-stained region (Fig. 2*B*), and it might be possible that GFP-Ker1p also localizes outside the nucleolus due to overproduction under the control of the strong *nmt1* promoter. For controls, we examined localization of GFP itself and observed a clear cytoplasmic distribution (Fig. 2, *D–F*). We also examined the localization of the nucleolar protein fibrillarin (GFP-fibrillarin) expressed in the same GFP fusion vector and found that it localized specifically in the crescent-shaped nucleolus (Fig. 2, *G–I*). As expected, the crescent-shaped region in the nucleus shows much lower DAPI staining in Fig. 2*G*. Taken together, we conclude from these results that Ker1p is predominantly localized in the nucleolus, although it is also possible that a certain fraction of Ker1p localizes in the nucleoplasm.

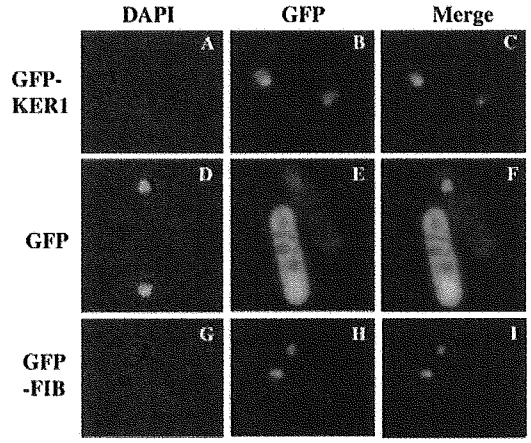

FIG. 2. **Ker1p predominantly localizes in the nucleolus.** The GFP-Ker1p (*GFP-KER1*; *A–C*) or GFP-fibrillarin (*GFP-FIB*; *G–I*) fusion protein or GFP alone (*D–F*) was expressed in *S. pombe* strain JY742. DNA was visualized by DAPI staining in *A*, *D*, and *G*. The localization of GFP fusion proteins and GFP is shown in *B*, *E*, and *H*. Merged images are shown in *C*, *F*, and *I*.

Co-immunoprecipitation of Ker1p and pol I—The apparent nucleolar localization of Ker1p prompted us to study the physical interaction of RPA21 (pol I) and Ker1p *in vivo*. Therefore, extracts prepared from cells expressing Ker1p-HA_3 were immunoprecipitated with anti-HA antibody (12CA5) beads, and coprecipitated proteins were detected by immunoblotting. Fig. 3*A* shows that pol I subunits RPA190, RPA140, and RPA21 co-immunoprecipitated with Ker1p, suggesting that Ker1p associates with pol I *in vivo*. The association is specific for pol I because the pol II subunit Rpb1 was not co-immunoprecipitated (Fig. 3*A*, *fourth panel*). Conversely, Ker1p co-immunoprecipitated with RPA140 and RPA21 when anti-RPA190 antibody was used for immunoprecipitation (Fig. 3*B*). These results confirm that Ker1p associates with pol I *in vivo*. No subunit was precipitated without the specific antibodies (*lane 3*). It should be noted that the bands of Ker1p again appeared to be doublets (*lane 2*), suggesting that the upper and lower bands correspond to the 32- and 30-kDa forms of the protein, respectively, as shown in Fig. 1*B*. The results suggest that pol I associates with both phosphorylated and non-phosphorylated Ker1p.

Ker1p Is Co-fractionated Biochemically with pol I—The above results suggest that Ker1p is a pol I subunit. To confirm biochemically that Ker1p is a novel pol I subunit, we purified pol I from an *S. pombe* strain (YI28) expressing both Ker1p-HA_3 and RPA140 tagged with a His_6-FLAG epitope. The whole cell extract was first affinity-purified using a nickel-agarose column and then fractionated by DEAE-Sephadex A25 column chromatography. We observed that Ker1p co-eluted with the peak fractions (fractions 13 and 14) of pol I detected through the RPA190 and RPA21 subunits (Fig. 4). Although more rigorous biochemical purification is needed, the elution pattern through the DEAE column confirms that Ker1p is a subunit of pol I. We noted that fractions 11 and 12 might also contain pol I without Ker1p and RPA21, but we did not examined these

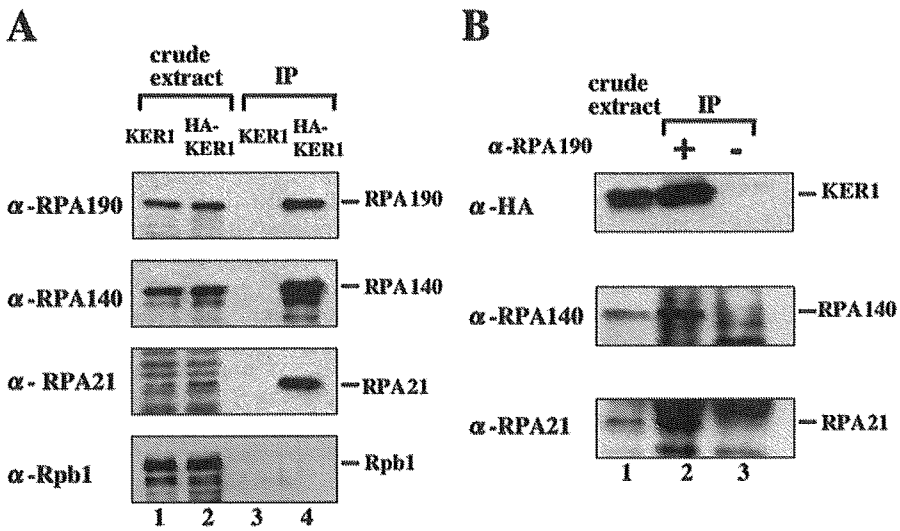

FIG. 3. **Ker1p associates with pol I.** *A*, extracts from strains IZ2 and YI28 expressing Ker1p (*KER1*) and Ker1p-HA_3 (*HA-KER1*), respectively, were immunoprecipitated with anti-HA monoclonal antibody (12CA5) beads. The extracts (*lanes 1* and *2*) and immunoprecipitates (*IP*; *lanes 3* and *4*) were subjected to SDS-PAGE, followed by immunoblot analysis with antibodies against RPA190, RPA140, RPA21, and Rpb1. 25 μg of crude extract was used for each control. *B*, extracts from strains expressing Ker1p-HA_3 were immunoprecipitated with anti-RPA190 antibody. The extract (*lane 1*), the immunoprecipitates with anti-RPA190 antibody (*lane 2*), and a sample without anti-RPA190 antibody treatment (*lane 3*) were subjected to SDS-PAGE, followed by immunoblot analysis with antibodies against HA, RPA140, and RPA21. The position of each band is indicated by the *bar* on the right of *A* and *B*. Ker1p appears as a doublet of bands. The dense bands seen at the top of the *third panel* (*lanes 2* and *3*) were derived from the light chain of immunoglobulin G.

fractions further in this study.

Genetic Interaction between Ker1p and RPA21—We have previously shown that overproduced Rrn3p is able to suppress the temperature-sensitive growth defect of *rpa21* mutants, indicating a genetic interaction between RPA21 and Rrn3p (41). To examine the genetic interaction between Ker1p and RPA21, we introduced a multicopy vector expressing Ker1p under the control of the CMV promoter into the three temperature-sensitive *rpa21* mutants (*ts152*, *ts296*, and *ts2817*) (41) and examined whether the growth defects of the mutants were suppressed at the restrictive temperature. As shown in Fig. 5, overproduction of Ker1p clearly suppressed the growth deficiency of the three mutants, indicating a genetic interaction between Ker1p and RPA21. Since A14 was shown previously to be required for stable association of A43 with pol I in *S. cerevisiae* (11), it appears that Ker1p is also required for stable association of RPA21 with pol I.

Ker1p Has a Limited Homology to S. cerevisiae A14—No apparent homologous protein was initially found when the Ker1p sequence was used in a data base search. However, the results obtained above clearly indicate that Ker1p is a pol I subunit and that it interacts with RPA21. Because RPA21 is an ortholog of A43 of *S. cerevisiae*, we re-examined the homology of Ker1p to *S. cerevisiae* A14, which heterodimerizes with A43. Previously, A14 was suggested to have homology to a putative open reading frame of IPF1568 from *Candida albicans* (11), suggesting that the A14 gene family is conserved in *C. albicans*, although no genetic or biochemical evidence was presented. This suggestion prompted us to directly investigate the homologies among Ker1p, A14, and IPF1568 (hereafter referred to as *C. albicans* A14), and Fig. 6 shows an alignment of these proteins constructed using ClustalW. We found that Ker1p shows 21% identity and 27% similarity to the 126-amino acid sequence of *S. cerevisiae* A14 and that the N-terminal 60 amino acids of Ker1p show especially high identity (37%) and similarity (43%) to *S. cerevisiae* A14. The N-terminal region also shows significant identity between the A14 subunits of *S. cerevisiae* and *C. albicans* (11), and Ker1p shows 26% identity and 36% similarity to the 132-amino acid sequence of *C. albicans* A14. The local identity of Ker1p to the *S. cerevisiae* and *C. albicans* A14 subunits is especially high (38 and 42%, respectively) between amino acids 42 and 65 of Ker1p, and this region contains a motif that may be conserved between the *S. cerevisiae* and *C. albicans* A14 subunits (SQLKRIQR), as already suggested by Peyroche *et al.* (11). We conclude from these results that Ker1p is an ortholog of A14 from both *S. cerevisiae* and *C. albicans*.

ker1$^+$ *Is Required for Growth Only at High Temperatures*—To examine whether *ker1*$^+$ is essential for cell growth, we replaced one of the chromosomal copies of *ker1*$^+$ with a disrupted *ker1*Δ::*ura4*$^+$ allele in the *S. pombe* diploid. A Ura$^+$ transformant (YI29) was chosen and subjected to tetrad analysis upon sporulation (Fig. 7*A*). Of the 20 asci dissected, one yielded four viable spores; seven yielded three viable spores; and the remaining 12 yielded two viable spores on yeast extract/peptone/dextrose medium plates at 30 °C. Large colonies were invariably Ura$^-$, whereas all of the small colonies, including the extremely small ones, were Ura$^+$. Correct disruption of the *ker1*$^+$ locus in the Ura$^+$ segregant YI30 was verified by PCR (data not shown). Growth of the colonies was tested at 25, 30, and 36 °C; none of the Ura$^+$ colonies grew at 36 °C, but all of the Ura$^-$ colonies did, indicating that *ker1*$^+$ is not essential for cell growth at 30 or 25 °C, but is required for cell growth at 36 °C (Fig. 7*B*).

*ker1*Δ *Is Suppressed by Overproduction of RPA21 or Rrn3p*—We subsequently examined whether complete deletion of *ker1*$^+$ (*ker1*Δ) is also suppressed by overproduction of RPA21. Fig. 8 shows that overexpression of RPA21 suppressed the growth defect of *ker1*Δ, again suggesting (see Fig. 5) that Ker1p is required for stable association of RPA21 with pol I. This result also suggests that RPA21 can associate with pol I independently of Ker1p. Because the rDNA-specific transcription factor Rrn3p interacts with RPA21 (41), we also examined

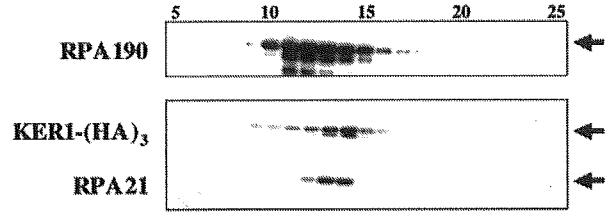

FIG. 4. **Ker1p co-fractionates with pol I.** Extracts from strains expressing Ker1p-HA$_3$ (*KER1-(HA)$_3$*) were loaded onto a nickel-agarose column. The eluted fractions were then loaded onto a DEAE-Sephadex A25 column and eluted with a linear gradient of 50–500 mM ammonium sulfate. Peaks of RPA190, RPA21, and Ker1p were detected by Western blotting using antibodies against RPA190, RPA21, and HA, respectively. The *numbers* indicate the *lanes*, and the *arrows* indicate RPA190, Ker1p-HA$_3$, and RPA21.

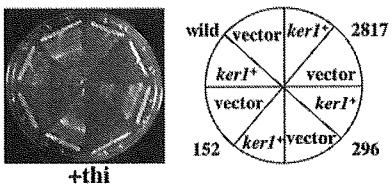

FIG. 5. **Overproduction of Ker1p suppresses the temperature-sensitive growth of three *rpa21* mutants.** Each of the temperature-sensitive mutants (*ts152*, *ts296*, and *ts2817*) transformed with pYI195 (*ker1*$^+$) or pAUR222 (*vector*) was re-streaked on minimal medium with thiamine (+*thi*) containing aureobasidin A and incubated for 5 days at 36 °C. *ker1*$^+$ was expressed under the control of the CMV promoter.

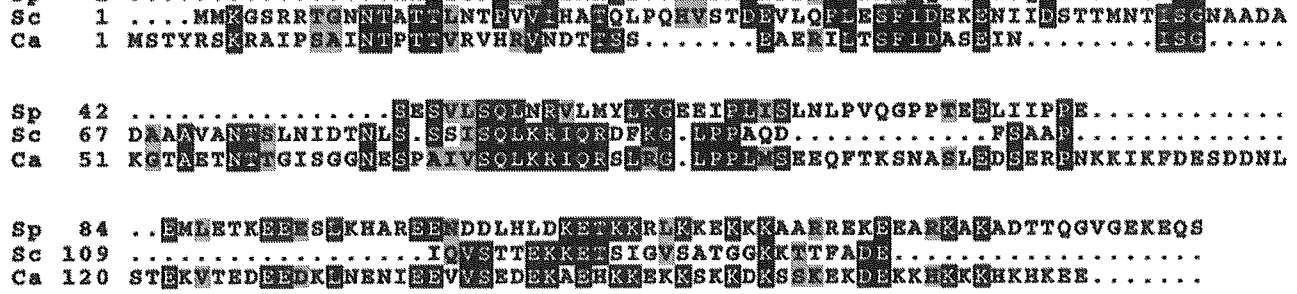

FIG. 6. **Amino acid sequence alignment of *S. pombe* Ker1p (*Sp*) with *S. cerevisiae* A14 (*Sc*) and *C. albicans* IPF1568 (*Ca*).** Identical and similar residues are highlighted in *black* and *gray*, respectively. The alignment was generated with the ClustalW program using the ID matrix. (The default BLOSUM matrix yielded a different alignment, in which Ker1p appeared to be less homologous to *S. cerevisiae* A14.)

whether overexpression of Rrn3p is able to suppress the temperature-sensitive growth of *ker1*Δ. As shown in Fig. 8, overproduction of Rrn3p suppressed the temperature-sensitive phenotype of *ker1*Δ, suggesting that Ker1p interacts with Rrn3p and directly stabilizes the association of Rrn3p with pol I. However, the alternative possibility remains that overproduced Rrn3p can interact with RPA21 and perhaps stabilize the association of RPA21 with pol I without the participation of Ker1p. Fig. 8 also shows that multiple copies of *rpa190*$^+$ were unable to suppress the *ker1*Δ phenotype.

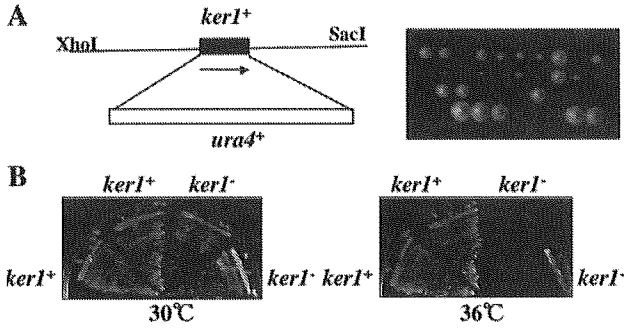

FIG. 7. **Gene disruption of *ker1*$^+$.** *A*: *left panel*, the 4.5-kb XhoI-SacI DNA fragment used for *ker1*$^+$ disruption; *right panel*, tetrads of diploids (*ker1*Δ::*ura4*$^+$/*ker1*$^+$) grown at 30 °C. *B*, growth of four haploid segregants derived from the ascospore produced by tetrad dissection of the *ker1*Δ::*ura4*$^+$/*ker1*$^+$ diploid.

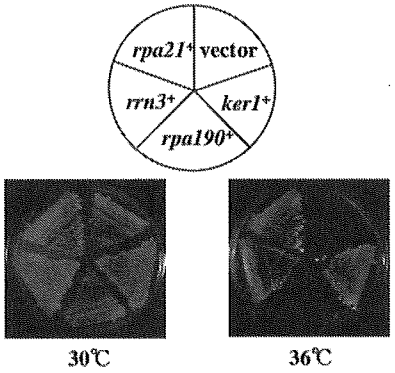

FIG. 8. **Temperature-sensitive growth of a *ker1*Δ strain is suppressed by overexpression of *rpa21*$^+$ or *rrn3*$^+$, but not *rpa190*$^+$.** *vector*, *ker1*$^+$, *rpa190*$^+$, *rrn3*$^+$, and *rpa21*$^+$ indicate strain YI28 (*ker1*Δ) carrying pREP41 (an empty vector), pYI210 (*ker1*$^+$), pGK100 (*rpa190*$^+$), pKI27 (*rrn3*$^+$), and pYI82 (*rpa21*$^+$). Each transformant was re-streaked on minimal medium plates without leucine and thiamine and incubated at 36 or 30 °C for 5 days.

Dissociation of Ker1p from pol I in Post-log-phase Cells—The data in Fig. 8 suggest that Ker1p is involved in stabilizing the association of Rrn3p with pol I, either directly or indirectly. Because Rrn3p is released from pol I in post-log-phase or growth-arrested cells (23, 24, 26), we examined whether Ker1p is also released from pol I, resulting in destabilization of Rrn3p in pol I in post-log-phase cells. As shown in Fig. 9, pol I from cells expressing Ker1p-HA$_3$ in mid- and post-log phase was immunoprecipitated with anti-RPA190 antibody, and the relative amounts of RPA190, RPA140, and Ker1p were compared. We observed a drastic decrease in the ratio of Ker1p (both phosphorylated and non-phosphorylated) to RPA190 in pol I prepared from post-log-phase cells (Fig. 9*A*, *right panels*, compare *lanes 2* and *3* with *lane 1*), although the ratio of RPA140 to RPA190 did not change significantly, suggesting that Ker1p is dissociated from pol I in the post-log phase. The dissociation of Ker1p from pol I may cause instability of Rrn3p in pol I, either directly or indirectly, resulting in dissociation of Rrn3p from pol I, which inactivates rDNA transcription.

DISCUSSION

In this study, we have shown that Ker1p isolated by a yeast two-hybrid system using RPA21 as bait is the counterpart of the *S. cerevisiae* pol I subunit A14. This is the first demonstration that a pol I-specific A14 ortholog is conserved in eukaryotes other than *S. cerevisiae*, despite no apparent homolog of A14 being identified in the *S. pombe* genome. We have successfully aligned the amino acid sequence of almost the entire length of Ker1p with those of A14 and IPF1568 (Fig. 6), indicating that these subunits are indeed grouped into a gene family. Our investigation of Ker1p has, however, also revealed features of Ker1p that are distinct from those of A14. First, Ker1p is phosphorylated (Fig. 1), whereas phosphorylation of

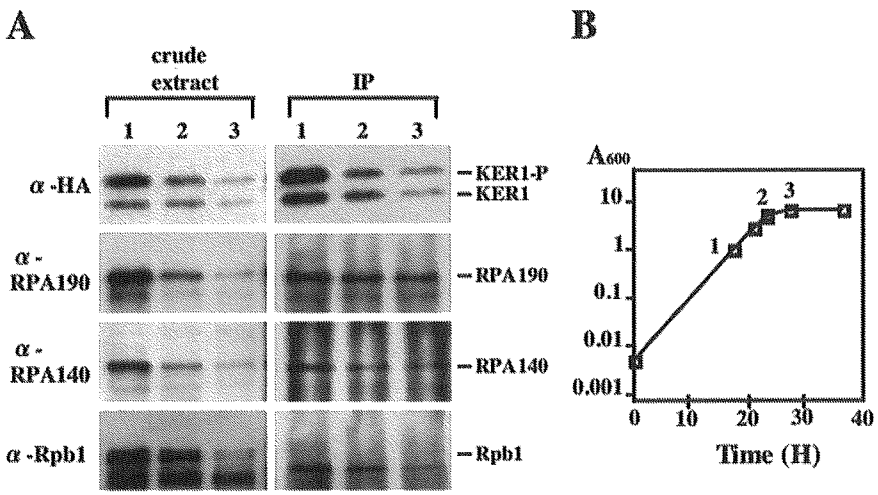

FIG. 9. **Dissociation of Ker1p from pol I in post-log-phase cells.** *A*, extracts were prepared from strain YI28 in mid-log-phase cells (*lane 1*) and post-log-phase cells (*lanes 2* and *3*) at the times indicated in *B*. *Left panels*, for detection of each subunit in the crude extract, 50 μg of each extract was loaded onto an SDS-polyacrylamide gel. Ker1p-HA$_3$, RPA190, RPA140, and Rpb1 (pol II for a control) were detected by immunoblot analysis with antibodies against HA, RPA190, RPA140, and Rpb1, respectively. *Right panels*, pol I in the crude extract was immunoprecipitated with anti-RPA190 antibody. The immunoprecipitates (*IP*) were subjected to SDS-PAGE, followed by immunoblot analysis with antibodies against HA, RPA190, RPA140, and Rpb1. We noted that bands detected by anti-Rpb1 antibody were nonspecific. *KER1-P*, phosphorylated Ker1p; *KER1*, Ker1p. *B*, strain YI28 was grown in yeast extract/dextrose medium at 30 °C. The culture was harvested at the indicated times (*time points 1*, *2*, and *3*). The A_{600} values of the culture at *time points 1*, *2*, and *3* were ~1.0 (mid-log phase), ~5.3, and ~6.8 (post-log phase), respectively. The doubling times at each point were ~2 h (*time point 1*), ~6 h (*time point 2*), and ~20 h (*time point 3*). In this study, we defined a temporary slow growth phase, such as those at *time points 2* and *3*, as a post-log phase.

TABLE II

Comparison of the pol I subunits of S. pombe and S. cerevisiae

The sequence data and identity were obtained as indicated: *rpa190*$^+$ (36, 37); *rpa140*$^+$ (GenBank™/EMBL accession number AL136535); *rpa42*$^+$ (38); *rpa17*$^+$ (39); *Sprpa12*$^+$ (40); *rpb5*$^+$, *rpb6*$^+$, *rpb8*$^+$, *rpb10*$^+$, and *rpb12*$^+$ (12); *rpa51*$^+$ (42); *rpa21*$^+$ (41); and *ker1*$^+$ (this work).

S. pombe		*S. cerevisiae*		Identity
Gene	No. of amino acids	Gene	No. of amino acids	
				%
rpa190$^+$	1689	*RPA190*	1664	50
rpa140$^+$	1228	*RPA135*	1203	63
rpa42$^+$	348	*RPC40*	335	58
rpa17$^+$	125	*RPC19*	142	63
Sprpa12$^+$	119	*RPA12*	125	55
rpb5$^+$	210	*RPB5*	215	56
rpb6$^+$	142	*RPB6*	155	54
rpb8$^+$	125	*RPB8*	146	39
rpb10$^+$	71	*RPB10*	70	72
rpb12$^+$	63	*RPB12*	70	39
rpa51$^+$	425	*RPA49*	415	30
rpa21$^+$	173	*RPA43*	326	36
ker1$^+$	147	*RPA14*	137	21
?		*RPA34*	233	

A14 has never been observed. Second, Ker1p is suggested to interact, either directly or indirectly, with Rrn3p and to stabilize the association of Rrn3p with pol I *in vivo* (Fig. 8), whereas it is unclear whether A14 affects the stability of Rrn3p with pol I *in vivo*. Third, Ker1p is released from pol I in post-log-phase cells (Fig. 9), whereas such instability of A14 in post-log-phase or growth-arrested cells is unknown in *S. cerevisiae*. The significance of these differences must await future studies to determine whether A14 can be phosphorylated or does dissociate from pol I in post-log-phase cells.

A comparison of the pol I subunits in *S. pombe* and *S. cerevisiae* is shown in Table II. 10 subunits constituting the core structure (RPA190, RPA140, RPA42, RPA17, Rpb5, Rpb6, Rpb8, Rpb10, Rpb12, and SpRPA12) are conserved from *S. cerevisiae* to *S. pombe* pol I. RPA190 and RPA140 were not examined, but seven of the remaining eight subunits (all except Rpb8) could substitute for the corresponding subunits in *S. cerevisiae*, suggesting functional conservation of most of the subunits (38–40, 49). In three specific subunits, including Ker1p, RPA51 was tested and found to rescue an *rpa49* mutation in *S. cerevisiae* (42). Although RPA21 encodes only 174 amino acids and appears to be much diversified from *S. cerevisiae* A43 (*S. cerevisiae* A43 contains 326 amino acids), its role in pol I recruitment to the rDNA promoter is conserved (41), and it is plausible that the N-terminal region conserved in the A43 gene family plays a role in the interaction with Rrn3p. The question of whether *S. pombe* pol I conserves a counterpart of *S. cerevisiae* A34.5 is unresolved. We believe that the primary sequence of the A34.5 homolog, if any such protein exists, may be poorly conserved in *S. pombe*. Mouse pol I has been found to contain distinct subunits from lower eukaryotes, such as PAF67 and PAF49 (33, 34, 50). These results tempt us to speculate that lower eukaryotes such as yeast might conserve the 14 subunits found in *S. cerevisiae* and that higher eukaryotes might have more specific subunits such as PAF67 and PAF49, in addition to the 14 conserved subunits.

It is known that A14 is not phosphorylated in *S. cerevisiae* pol I (1, 51, 52), whereas here Ker1p was found to be phosphorylated, suggesting that specific subunit phosphorylation has also evolved independently among pol I subunits. Indeed, *S. cerevisiae* A43 is multiphosphorylated (53), whereas mammalian A43 is barely phosphorylated (24). It has been argued that A43 must be phosphorylated to associate with Rrn3p in *S. cerevisiae*, whereas Rrn3p phosphorylation is a prerequisite for the association of A43 with Rrn3p in mammalian cells (24, 53, 54). In this context, the functional dissection of Ker1p phosphorylation/dephosphorylation may provide a novel insight into the pol I recruitment mechanism.

It appears that Ker1p is required for the stability of RPA21 based on multicopy suppression experiments. (i) *ker1*Δ exhibits a temperature-sensitive growth deficit, and the temperature-sensitive deficit is suppressed by overproduction of RPA21 (Fig. 8). (ii) The temperature-sensitive growth deficit of three *rpa21* mutants (*ts152*, *ts296*, and *ts2817*) is suppressed by overexpression of *ker1*$^+$ (Fig. 5). Since it is known that A14 is also required for the stability of A43 in *S. cerevisiae* (9, 11), the role of Ker1p may be, as expected, similar to that of A14. To verify the Ker1p function, purification of pol I from extracts of *ker1*Δ mutants deserves future study. Unexpectedly, as shown in Fig. 8, overproduction of Rrn3p also suppresses the temperature-sensitive phenotype of the *ker1*Δ mutant, suggesting that Ker1p is also required for the stable association of Rrn3p with pol I. Alternatively, these suppression data could suggest that overproduction of Rrn3p suppresses the instability of RPA21 in pol I without participation of Ker1p, leading to indirect suppression of the temperature-sensitive phenotype of *ker1*Δ. Clearly, future biochemical experiments are required to reveal whether Rrn3p directly interacts with Ker1p.

Accumulating evidence has shown that dissociation of Rrn3p from pol I in post-log-phase or growth-arrested cells causes a decrease in pol I recruitment to the promoter, resulting in a decrease in or halting of rDNA transcription. As described above, it has been argued that post-translational modification (phosphorylation/dephosphorylation) of A43 and Rrn3p regulates the stability of the pol I-Rrn3p complex, causing dissociation of Rrn3p from pol I in post-log-phase or growth-arrested cells. The immunoprecipitation experiments in Fig. 9, performed using anti-RPA190 antibody, showed that the amounts of both forms of Ker1p (phosphorylated and non-phosphorylated forms) relative to RPA140 and RPA190 are reduced drastically after cells enter the post-log phase. The results suggest that dissociation of Ker1p from pol I in post-log-phase cells is one of the regulatory mechanisms of Rrn3p dissociation from pol I since the dissociation of Ker1p may lead to instability of RPA21 and Rrn3p in pol I. It is also possible that release of Ker1p induces certain modification(s) of RPA21 and Rrn3p that result in release of Rrn3p from pol I. Therefore, it is tempting to speculate that the association/dissociation of Ker1p might primarily regulate growth-dependent transcription of rDNA in *S. pombe*.

Acknowledgments—We acknowledge the Resource Center/Primary Database of the German Human Genome Project for sending us a cosmid including *rrn3*$^+$. We thank L. Pape (University of Wisconsin) for communicating the results of a homology search for Ker1p. We also acknowledge Akio Toh-e (University of Tokyo) for critical reading of the manuscript.

REFERENCES

1. Thuriaux, P., and Sentenac, A. (1992) in *The Molecular and Cellular Biology of the Yeast Saccharomyces* (Jones E. W., Pringle J. R., and Broach J. R., eds) Vol. 2, pp. 1–48, Cold Spring Harbor Laboratory, Cold Spring Harbor, NY
2. Armache, K. J., Kettenberger, H., and Cramer, P. (2003) *Proc. Natl. Acad. Sci. U. S. A.* **100,** 6964–6968
3. Bushnell, D. A., and Kornberg, R. D. (2003) *Proc. Natl. Acad. Sci. U. S. A.* **100,** 6969–6973
4. Bischler, N., Brino, L., Carles, C., Riva, M., Tschochner, H., Mallouh, V., and Schultz, P. (2002) *EMBO J.* **21,** 4136–4144
5. Edwards, A. M., Kane, C. M., Young, R. A., and Kornberg, R. D. (1991) *J. Biol. Chem.* **266,** 71–75
6. Thuriaux, P., Mariotte, S., Buhler, J. M., Sentenac, A., Vu, L., Lee, B. S., and Nomura, M. (1995) *J. Biol. Chem.* **270,** 24252–24257
7. Liljelund, P., Mariotte, S., Buhler, J. M., and Sentenac, A. (1992) *Proc. Natl. Acad. Sci. U. S. A.* **89,** 9302–9305
8. Gadal, O., Mariotte-Labarre, S., Chedin, S., Quemeneur, E., Carles, C., Sentenac, A., and Thuriaux, P. (1995) *Mol. Cell. Biol.* **17,** 1787–1795
9. Smid, A., Riva, M., Bouet, F., Sentenac, A., and Carles, C. (1995) *J. Biol. Chem.* **270,** 13534–13540

10. Peyroche, G., Milkereit, P., Bischer, N., Tschochner, H., Schultz, P., Sentenac, A., Carles, C., and Riva, M. (2000) *EMBO J.* **19,** 5473–5482
11. Peyroche, G., Levillain, E., Siaut, M., Callebaut, I., Schultz, P., Sentenac, A., Riva, M., and Carles, C. (2002) *Proc. Natl. Acad. Sci. U. S. A.* **99,** 14670–14675
12. Sakurai, H., Mitsuzawa, H., Kimura, M., and Ishihama, A. (1999) *Mol. Cell. Biol.* **19,** 7511–7518
13. Siaut, M., Zaros, C., Levivier, E., Ferri, M. L., Court, M., Werner, M., Callebaut, I., Thuriaux, P., Sentenac, A., and Conesa, A. (2003) *Mol. Cell. Biol.* **23,** 195–203
14. Todone, F., Brick, P., Werner, F., Weinzierl, R. O. J., and Onesti, S. (2001) *Mol. Cell* **8,** 1137–1143R. O. J.
15. Sheffer, A., Varon, M., and Choder, M. (1999) *Mol. Cell. Biol.* **19,** 2672–2680
16. Lanzendorfer, M., Smid, A., Klinger, C., Schultz, P., Sentenac, A., Carles, C., and Riva, M. (1997) *Genes Dev.* **11,** 1037–1047
17. Orlicky, S., Tran, P. T., Sayre, M. H., and Edwards, A. M. (2001) *J. Biol. Chem.* **276,** 10097–10102
18. Meka, H., Daoust, G., Arnvig, K. B., Werner, F., Brick, P., and Onesti, S. (2003) *Nucleic Acids Res.* **31,** 4391–4400
19. Ferri, M. L., Peyroche, G., Siaut, M., Lefebvre, Q., Carles, C., Conesa, C., and Sentenac, A. (2000) *Mol. Cell. Biol.* **20,** 488–495
20. Moss, T., and Stefanovsky, V. Y. (2002) *Cell* **109,** 545–548
21. Ju, Q., and Warner, J. R. (1994) *Yeast* **10,** 151–157
22. Zaragoza, D., Ghavidel, A., Heitman, J., and Schultz, M. (1998) *Mol. Cell. Biol.* **18,** 4463–4470
23. Bodem, J., Dobreva, G., Hofmann-Rohrer, U., Iben, S., Zentgraf, H., Delius, H., Vingron, M., and Grummt, I. (2000) *EMBO Rep.* **1,** 171–175
24. Cavanaugh, A. H., Hirschler-Laszkiewicz, I., Hu, Q., Dundr, M., Smink, T., Misteli, T., and Rothblum, L. I. (2002) *J. Biol. Chem.* **277,** 27423–27432
25. Yamamoto, R. T., Nogi, Y., Dodd, J. A., and Nomura, M. (1996) *EMBO J.* **15,** 3964–3973
26. Milkereit, P., and Tschochner, H. (1998) *EMBO J.* **17,** 3692–3703
27. Keener, J., Josaitis, C. A., Dodd, J. A., and Nomura, M. (1998) *J. Biol. Chem.* **273,** 33795–33802
28. Miller, G., Panov, K. I., Friedrich, J. K., Trinkle-Mulcahy, L., Lamond, A. I., and Zomerdijk, J. C. B. M. (2001) *EMBO J.* **20,** 1373–1382J. C. B. M.
29. Claypool, J. A., French, S. L., Johzuka, K., Eliason, K., Vu, L., Dodd, J. A., Beyer, A. L., and Nomura, M. (2004) *Mol. Biol. Cell* **15,** 946–956
30. Grummt, I. (2003) *Genes Dev.* **17,** 1691–1702
31. Woychik, N. A. (1998) *Cold Spring Harbor Symp. Quant. Biol.* **63,** 311–317
32. Hu, P., Wu, S., Sun, Y., Yuan, C., Kobayashi, R., Myers, M. P., and Hernandez, N. (2003) *Mol. Biol. Cell* **22,** 8044–8055
33. Seither, P., Iben, S., Thiry, M., and Grummt, I. (2001) *Biol. Chem.* **382,** 1163–1170
34. Yamamoto, K., Yamamoto, M., Hanada, K., Nogi, Y., Matsuyama, T., and Muramatsu, M. (2004) *Mol. Cell. Biol.* **24,** 6525–6535
35. Alfa, C., Fantes, P., Hyams, J., McLeod, M., and Warbrick, E. (1993) *Experiments with Fission Yeast*, Cold Spring Harbor Laboratory , Cold Spring Harbor, NY
36. Yamagishi, M., and Nomura, M. (1988) *Gene (Amst.)* **74,** 503–515
37. Hirano, T., Konoha, G., Toda, T., and Yanagida, M. (1989) *J. Cell Biol.* **108,** 243–253
38. Imazawa, Y., Imai, K., Fukushima, A., Hisatake, K., Muramatsu, M., and Nogi, Y. (1999) *Mol. Gen. Genet.* **262,** 749–757
39. Imai, K., Imazawa, Y., Yao, Y., Yamamoto, K., Hisatake, K., Muramatsu, M., and Nogi, Y. (1999) *Mol. Gen. Genet.* **261,** 364–373
40. Imazawa, Y., Imai, K., Yao, Y., Yamamoto, K., Hisatake, K., Muramatsu, M., and Nogi, Y. (2001) *Mol. Gen. Genet.* **264,** 852–859
41. Imazawa, Y., Hisatake, K., Nakagawa, K., Muramatsu, M., and Nogi, Y. (2002) *Genes Genet. Syst.* **77,** 147–157
42. Nakagawa, K., Hisatake, K., Imazawa, Y., Ishiguro, A., Matsumoto, M., Pape, L., Ishihama, A., and Nogi, Y. (2003) *Genes Genet. Syst.* **78,** 199–209
43. Sherman, F., Fink, G. R., and Hicks, J. B. (1986) *Laboratory Course Manual for Methods in Yeast Genetics*, pp. 163–167, Cold Spring Harbor Laboratory, Cold Spring Harbor, NY
44. Harper, J. W., Adami, G. R., Wei, N., Keyomarsi, K., and Elledge, S. J. (1993) *Cell* **75,** 805–816
45. Mitsuzawa, H., Seino, H., Yamao, F., and Ishihama, A. (2001) *J. Biol. Chem.* **276,** 17117–17124
46. Ishiguro, A., Nogi, Y., Hisatake, K., Muramatsu, M., and Ishihama, A. (2000) *Mol. Cell. Biol.* **20,** 1263–1270
47. Sawin, K. E., and Nurse, P. (1996) *Proc. Natl. Acad. Sci. U. S. A.* **94,** 15146–15151
48. Oakes, M., Nogi, Y., Clark, M. W., and Nomura, M. (1993) *Mol. Cell. Biol.* **13,** 2441–2455
49. Shpakovski, G. V., Gadal, O., Labarre-Mariotte, S., Lebedenko, E. N., Miklos, I., Sakurai, H., Proshkin, S. A., Van Mullem, V., Ishihama, A., and Thuriaux, P. (2000) *J. Mol. Biol.* **295,** 1119–1127
50. Yuan, X., Zhao, J., Zentgraf, H., Hommer-Rohrer, U., and Grummt, I. (2002) *EMBO Rep.* **3,** 1082–1087
51. Buhler, J. M., Iborra, F., Sentenac, A., and Fromageot, P. (1976) *FEBS Lett.* **71,** 37–41
52. Breant, B., Buhler, J. M., Sentenac, A., and Fromageot, P. (1983) *Eur. J. Biochem.* **130,** 247–251
53. Fath, S., Milkereit, P., Peyroche, G., Riva, M., Carles, C., and Tschochner, H. (2001) *Proc. Natl. Acad. Sci. U. S. A.* **98,** 14334–14339
54. Zao, J., Yuan, X., Frodin, M., and Grummt, I. (2003) *Mol. Cell* **11,** 405–413
55. Waddel, S., and Jenkins, J. R. (1995) *Nucleic Acids Res.* **23,** 1836–1837
56. Basi, G., Schmid, E., and Maundrell, K. (1993) *Gene (Amst.)* **123,** 131–136